SECTION I
RESEARCH IN PROGRESS

NUCLEAR REACTIONS -- EXPERIMENTAL

HIGH ENERGY GAMMA RAY-PROTON CORRELATIONS

A.R. Lampis, J. Stevenson, W. Benenson, C. Bloch, D. Cebra, J. Clayton, D. Fox,
E. Kashy, D. Morrissey , M. Samuel, R. Smith, A. Tam, G. Westfall, K. Wilson, J. Winfield,

High energy gamma ray (20<E<120 MeV) production in heavy ion collisions has been studied by several groups[1-5]. The main features of the gamma spectra are the exponentially decreasing energy spectra and a slightly forward peaked angular distribution. The spectra are consistent with isotropic emission in a frame moving close to the nucleon-nucleon center-of-mass velocity.

The theories proposed to explain the gamma ray production mechanism include: nucleus-nucleus bremsstrahlung[6-8], neutron-proton bremsstrahlung[9], and statistical decay[10-11].

We report here results from a coincidence experiment between gamma rays (20-120 MeV) and protons (30-135 MeV), produced in collisions of E/A=40 MeV ^{14}N+Zn. The experiment was performed at the National Superconducting Cyclotron Laboratory, using the K500 cyclotron. Light charged particles (Z=1,2) were detected with 16 phoswich ΔE-E telescopes. The detectors were grouped in pairs and covered the angular range from 30° to 130°. Two gamma ray telescopes, consisting of a passive lead converter followed by a thin scintillator and a stack of 8 Cerenkov elements, were located at 60° (D1) and 120° (D2) in plane with the charged particle detectors but on the opposite side of the beam.

The gamma ray spectra taken in coincidence with protons look similar to the inclusive gamma ray spectra. In order to study the coincidence data in detail it is useful to take the ratio of the coincidence to singles cross-sections. This ratio R is defined in eqn.1

$$1) \quad R=\frac{\sigma_{\gamma\, p}}{\sigma_{\gamma}\ \sigma_{p}} \quad , \quad \sigma_{\gamma p}=\frac{d\sigma}{d\Omega_{\gamma} d\Omega_{p}} , \quad \sigma_{\gamma}=\frac{d\gamma}{d\Omega_{\gamma}} \quad , \quad \sigma_{p}=\frac{d\sigma}{d\Omega_{p}}$$

Fig. 1 shows the ratio R as a function of proton lab angle. The ratio R is roughly independent of detected proton lab angle and has a value of 0.6 barn^{-1}. These values can be compared with the proton-proton coincidence ratio of 0.35-0.6 barn^{-1} for ^{12}C+Ag at 40 MeV/n.[12]

In order to study how the ratio varies as a function of proton energy we added together the data from the four most forward ΔE-E detectors. The ratio R(E_p) is defined in eqn. 2 and is now

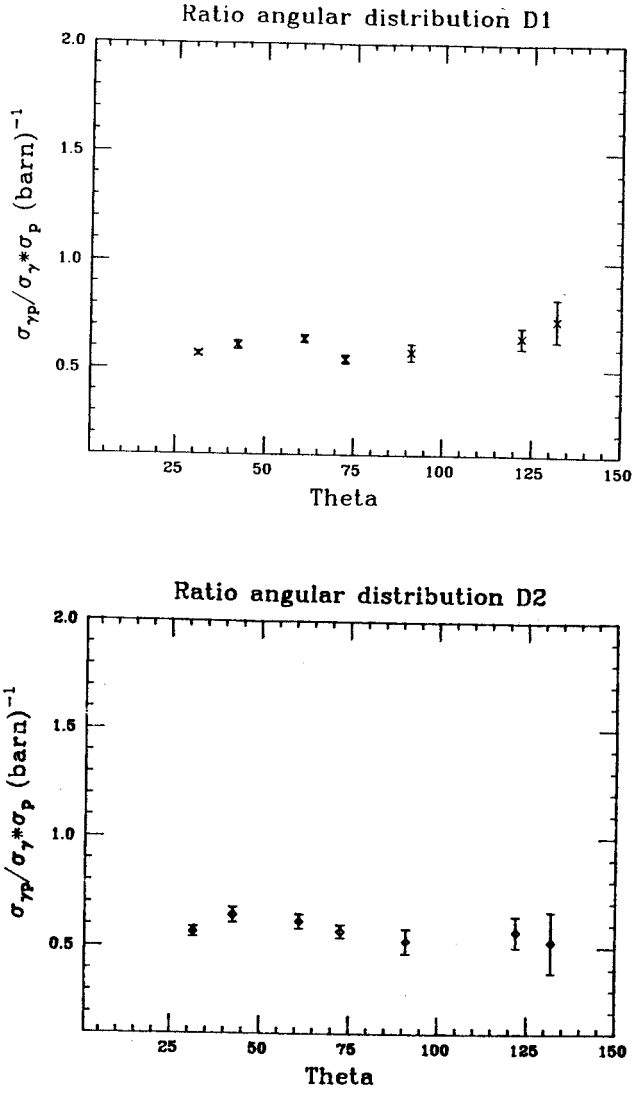

Fig 1. Angular distribution of the ratio (eq. 1) as a function of the ΔE-E angular position. 1a: gamma rays are detected in D1(60°) 1b: gamma rays are detected in D2(120°).

a function of proton energy rather than integrated over all proton energies.The ratio $R(E_p)$ is shown in Fig. 2 for the gamma ray detector at 60°. The ratio is essentially independent of proton energy.

$$2)\quad R(E_p)=\frac{\sigma_{\gamma p}(E_p)}{\sigma_\gamma\sigma_p(E_p)}\ ,\ \sigma_{\gamma p}=\frac{d^3\sigma}{d\Omega_\gamma d\Omega_p dE_p},$$

$$\sigma_\gamma=\frac{d\sigma}{d\Omega_\gamma}\ ,\ \sigma_p=\frac{d^2\sigma}{dE_p d\Omega_p}$$

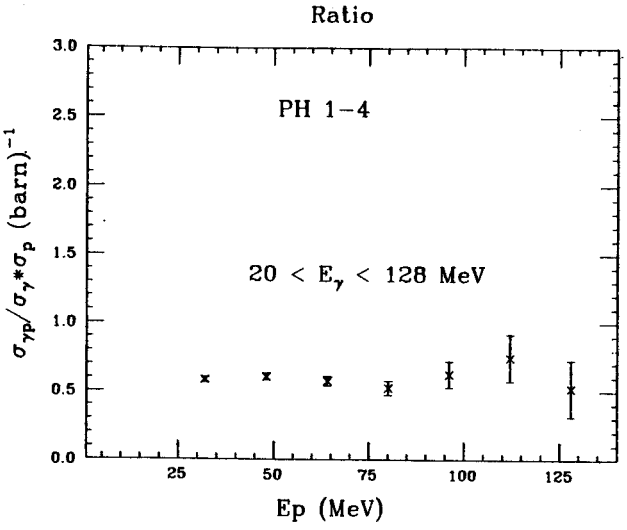

Fig. 2. Ratio (eq. 2) as a function of proton energy. Gamma ray energy is between 20 and 128 MeV.

A moving thermal source parameterization of the proton spectra for both singles and coincidence data was used. The source velocities listed in Table 1 are quite similar for the two data sets.

TABLE 1

p-singles	β=0.145
p-γ (D1)	β=0.140
p-γ (D2)	β=0.135

The gamma ray (D1) energy dependence of the ratio was studied by constructing the ratio $R(E_\gamma)$ defined in eqn 3.

$$3)\quad R(E_\gamma)=\frac{\sigma_{\gamma p}(E_\gamma)}{\sigma_\gamma(E_\gamma)\sigma_p}\ ,\ \sigma_{\gamma p}=\frac{d^3\sigma}{dE_\gamma d\Omega_\gamma d\Omega_p}$$

$$\sigma_\gamma=\frac{d^2\sigma}{d\Omega_\gamma dE_\gamma}\ ,\ \sigma_p=\frac{d\sigma}{d\Omega_p}$$

The ratio $R(E_\gamma)$ is shown in Fig. 3 for several different lower cutoffs for the proton energy. Again within experimental errors no variation is seen in the ratio.

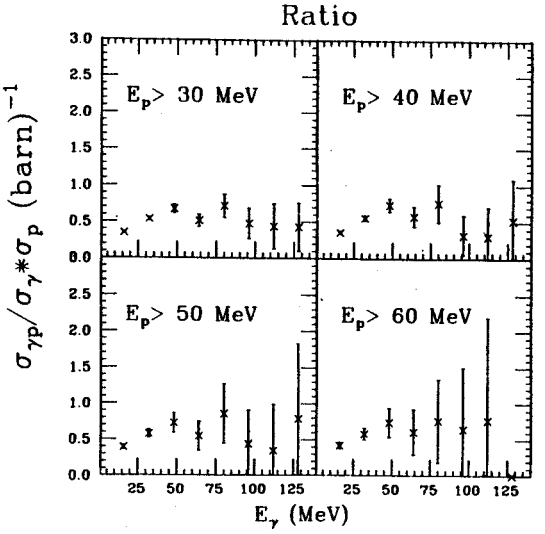

Fig. 3. Ratio (eq. 3) as a function of gamma ray energy for lower energy cutoffs of 30,40,50,60 MeV in proton energy.

Recent BUU calculations have predicted that the impact parameter dependence of the gamma yield is proportional to the overlap area of the colliding nuclei[9]. The overlap area, A(b), of the projectile and target nuclei is calculated assuming the nuclei to be spheres with radii $R=1.2*A^{1/3}$fermi. The coincidence to singles ratio can be calculated by assuming that the proton and gamma ray cross sections are both proportional to A(b). We calculated the ratio R assuming these proportionalities:

$$\sigma_\gamma \propto A(b) \quad \sigma_p \propto A(b) \quad \sigma_{\gamma p} \propto A(b)A(b)$$

so that:

$$4) \quad R = \frac{\int [A(b)]^2 db}{[\int A(b) db]^2}$$

We also considered an impact parameter dependence proportional to the overlap volume of the two nuclei (Table 2). The values of the ratio calculated with this simple model are about 50% larger then the experimental ones for both p-γ and p-p coincidence.

TABLE 2

	$^{14}N + ^{65}Zn (barn^{-1})$	$^{12}C + ^{107}Ag (barn^{-1})$
AREA	0.90	0.71
VOLUME	1.00	0.77
AR+VOL	0.95	0.74
EXP	0.6	0.35 - 0.6

In conclusion, we find that the ratio between the γ-p coincidence cross section and the gamma and proton singles cross sections is independent of both gamma ray and proton angle and does not vary with proton or gamma ray energy.

References

1. J. Stevenson et al., Phys. Rev. Lett. 57, 555 (1986).
2. E. Grosse et al., Europhys. Lett. 2,9 (1986)
3. N. Alamanos et al., Phys. Lett. 175B, 125 (1986).
4. M. Kwato Njock et al., Phys. Lett. 175B, 125 (1986)
5. R. Hingmann et al., Phys. Rev. Lett. 58, 759 (1987)
6. C.M. Ko, G. Bertsch and J. Aichelin, Phys Rev C31 (1985) 2324.
7. E.M. Nyaman, Phys. Lett. 136B (1984) 143
8. D. Vasak et al., Nucl. Phys A428 (1984) 291c
9. W. Bauer, G. Bertsch, W.Cassing, U. Mosel Phys. Rev C 34 (1986) 2127
10. H. Nifenecker and J.P. Bondorf, Nucl. Phys. A442 (1985) 478.
11. D. Fox private communication.

NEUTRON EMISSION FROM HEAVY-ION COLLISIONS

F. Deak[a], A. Galonsky, C.K. Gelbke, L. Heilbronn, J. Kasagi[b], A. Kiss[a], S. Langer, W. Lynch, T. Murakami, B. Remington[c], H.R. Schelin[d], Z. Seres[e] and M.B. Tsang

When a light fragment produced in a heavy-ion collision particle decays from a discrete unbound state the mode of particle emission is not described by thermal emission[1]. In recent experiments involving the study of nuclear mechanisms via neutron emission it was found that the dominant source of neutrons in a colinear geometry (target, fragment and neutron detector lined up) was the decay of a few low-lying, neutron-unbound, excited states of a fragment. For example, in the case $^{13}C^{*} \rightarrow ^{12}C$ + n we saw four obvious peaks at ±0.5 cm/ns and at ±2 cm/ns when constructing relative velocity spectra. The peaks at ±0.5 cm/ns arise from the 114-keV decay of the 9.5-MeV state of ^{13}C to the 4.4-MeV state of ^{12}C. The peaks at ± 2 cm/ns have the following origins. The 6.87-MeV state of ^{13}C (first neutron-unbound state) emits a 1.9-MeV neutron and the next three states emit neutrons of 0.6 to 0.8 MeV higher energy. In order to deduce a nuclear temperature from a Boltzmann population distribution, we need at least two discrete neutron-unbound states of the nucleus. The work would then be more convincing if we could resolve some of the levels around 2 cm/ns. There are many experimental effects that contribute to the size and width of a peak, such as, the width of the excited state, the isotopic mass resolution of the fragment detector, the timing resolution of the neutron detector (including the energy dependence of its thickness), the angular acceptance of the neutron and fragment detectors and the target thickness. The last three also affect the counting rate. All these effects have been put into a Monte Carlo code to help us design the experiment with better resolution. The colinear geometry was maximized by using a bank of seven silicon telescopes in line with a bank of seven neutron detectors a few meters behind the telescopes.

With these improvements, we measured neutron spectra in coincidence with light fragments resulting from collisions of ^{14}N projectiles at 35 MeV per nucleon with a Ag target at the K500 cyclotron. The fragments were detected using ΔE-E silicon telescopes placed at lab. angles Θ_F = 15° (out of plane), -15°, -30° (bank of seven), -64° (bank of seven) and -83° relative to the beam axis. Liquid scintillator detectors (NE213 or BICRON 501) were employed to detect the coincident neutrons, and the method of time-of-flight was used to determine the neutron energies. The detectors where placed at lab. angles Θ_n = -15° (bank of three), -30° (bank of seven), -64° (bank of seven), -115°, 15°, 31°, 60°, 110° and 160°, relative to the beam axis. The last six detectors were included to measure the complete angular distribution of neutrons in coincidence with fragments, not only in colinear geometry with fragments. We also measured angular distributions for neutron singles and for fragment singles. A bank of seven scintillator detectors is shown in Fig. 1, and a bank of silicon telescopes is shown in Fig. 2. Ten of the scintillator detectors were built for this experiment and we used Bicron 501 as liquid scintillator material. When tested in time calibration with a ^{60}Co source and also for n/γ discrimination, they had the same behavior as the NE213. The FWHM of the target gamma-ray peak was about 1.3 ns. Neutrons were distinguished from gamma-rays by pulse shape discrimination using two QDC's.

Fig. 1. A bank of seven scintillator detectors.

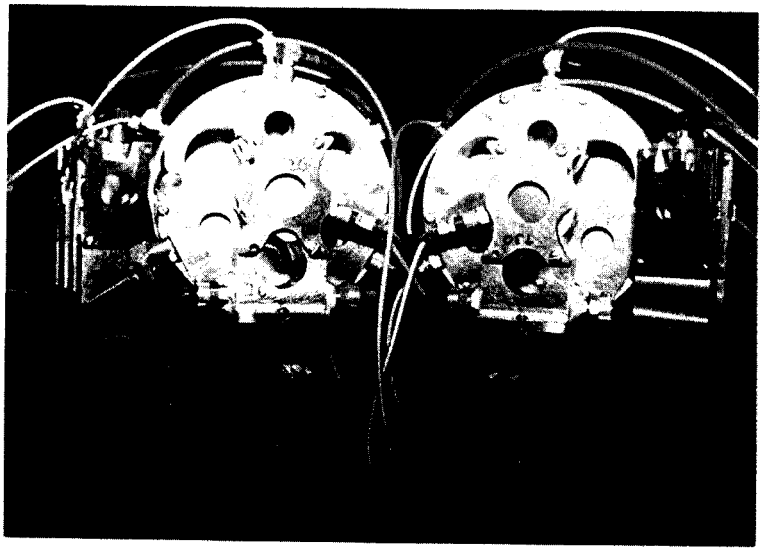

Fig. 2. The Si telescope arrangement.

a. Eötvös University, Budapest, Hungary.
b. Tokyo Inst. Technology, Japan.
c. Lawrence Livermore Lab.
d. On leave from Centro Tecnico Aeroespacial and (FAPESP), Brazil.
e. Central Research Lab., Budapest, Hungary.References

References

1. A. Kiss, F. Deak, Z. Seres, G. Caskey, A. Galonsky, L. Heilbronn, B. A. Remington and J. Kasagi, Phys. Lett. B 184,139(1987).

D.A. Cebra, W. Benenson, Y. Chen, R. Helmer[a], E. Kashy, R. Korterling[b], D.J. Morrissey, A. Pradhan, R.S. Tickle[c], G.D. Westfall, W.K. Wilson and A. VanderMolen

It is believed that the collision between two nuclei at incident energies greater than the Fermi energy creates an equilibrated hot zone in the interaction region. This concept was put forward with the introduction of the fireball model, which used the properties of an expanding gas of nucleons to reproduce the kinetic energy spectra of light nuclei (Z=1 and 2).[1,2] The slope parameter of the kinetic energy spectra was taken to be the temperature of the thermal region. The original experiments in this field were performed at relativistic energies, and refinements of the basic model were made as the measurements were extended into the intermediate energy regime and the fitting of the kinetic energy spectra extended to higher masses.[3] It became necessary to include three thermal sources, the target remnant, the fireball, and the projectile remnant. Each source has a characteristic temperature and emits particles isotropically in its rest frame.

If one assumes that these sources consist of gases of nucleons that have reached statistical equilibrium, one would expect that other methods of measuring the source temperature should yield results similar to those suggested by the slope parameters of the various contributions to the kinetic energy spectra. One other method of testing the existence of a thermalized zone is to determine the temperature of the source of charged particles by measuring the relative populations of excited states in the intermediate mass fragments produced in the collision. If the source is in thermal equilibrium, the ratio of two states of an isotope will be given by the Boltzmann distribution. For the system 35 Mev/nucleon ^{14}N + Ag, measurements of the ratio between the first excited state and ground state in isotopes of lithium and beryllium yielded temperatures an order of magnitude lower than those suggested by the slope of the energy spectra.[4] In order to compensate for the preferential feeding of the ground state by the decay of particle unbound states of heavier fragments, the measurements of the ratios of excited states were extended to higher lying unstable states.[5,6,7,8]

The majority of the experiments described above studied the ^{14}N + Ag system at E/A = 35 MeV. One of the difficulties noted in these earlier studies of the ratios of particle unbound states was that the extracted temperature was a function of the angle at which the measurement was made. This dependence on angle is caused by the differing contributions to the production cross-sections for light particles by the different sources as a function of angle. In order to eliminate any effects caused by the interactions between the various sources, we performed an experiment to study the system 500 MeV p + Ag at the Tri-University Meson Facility in Vancouver, British Columbia. This system has the same target and the same total beam energy as the 35 MeV/nucleon ^{14}N + Ag experiments. One would expect that a similar amount of energy would be deposited within the target nucleus, but that there would be no creation of an intermediate velocity thermal source, and the projectile remnant would not be capable of decay. Thus the charged particles which are emitted from this reaction would all come from the thermalized zone within the target itself.

In order to measure the ratios of particle unstable excited states, it is necessary to detect both of the particles associated with the

decay of the original fragment. The excitation energy of the state can be determined from the relative momentum between the two particles. We used a large solid angle (165 msr) three plane multi-wire proportional chamber (MWPC) to determine to positions of the particles emitted from the reaction. The MWPC had a position resolution of 5mm in the x and y planes (angular resolution of 0.7°). The third plane was used to resolve ambiguities that arise when several particles hit the detector simultaneously. Behind the MWPC was a four-by-four stacked array of fast/slow plastic scintillator phoswich detectors. These detectors had a 1.6 mm fast plastic delta E scintillator and a 127 mm slow plastic stopping scintillator. By separating the light produced in the two scintillators and comparing the signals one can get information about the particle's total energy, mass and charge (for particles up to Z=2).

In order to calibrate the light particle detectors, we ran beams of 500, 320, and 200 MeV protons on targets of CH_2 and CD_2. A coincidence was demanded with a forward angle scintillator, and the scattering angle of the particle hitting the detector to be calibrated was determined by the MWPC. For elastically scattered protons from hydrogen or deuterium in the target, the energy is determined by the scattering angle. The range of beam energies and targets was designed to create a range of energies of elastically scattered protons comparable to the energy range to which the detectors are sensitive. Figure 1 shows a plot of light produced in the stopping scintillator against the energy of the elastically scattered particle.

The kinetic energy spectra for protons are displayed in figure 2. The low energy cut was determined by the minimum energy necessary to penetrate the delta E scintillator, and the high energy cut was determined by the energy at which we could no longer distinguish the different isotopes of hydrogen. The ΔP correlations will

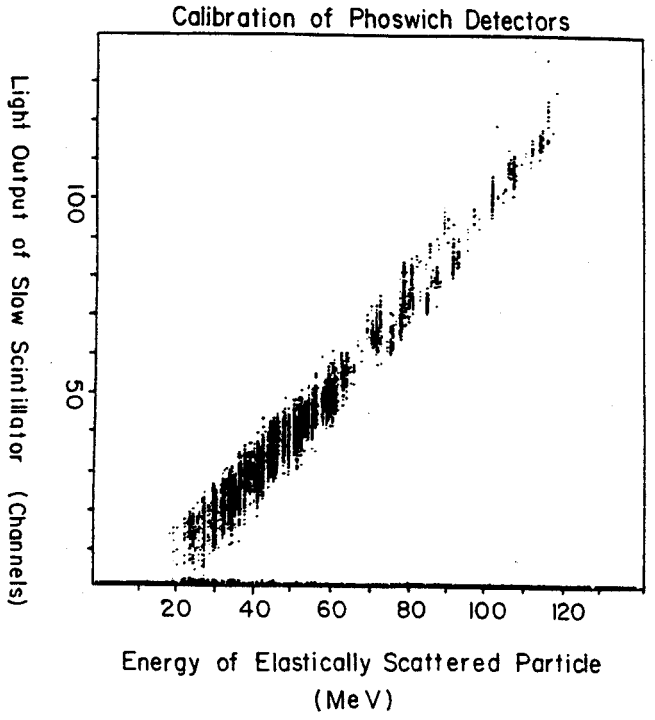

Fig. 1. Corrected light produced in the stopping (slow) scintillator plotted against the energy of the elastically scattered proton. Energy is determined by the scattering angle, beam energy and target. Calibrations included 500, 320, and 200 MeV p + CH_2 and CD_2.

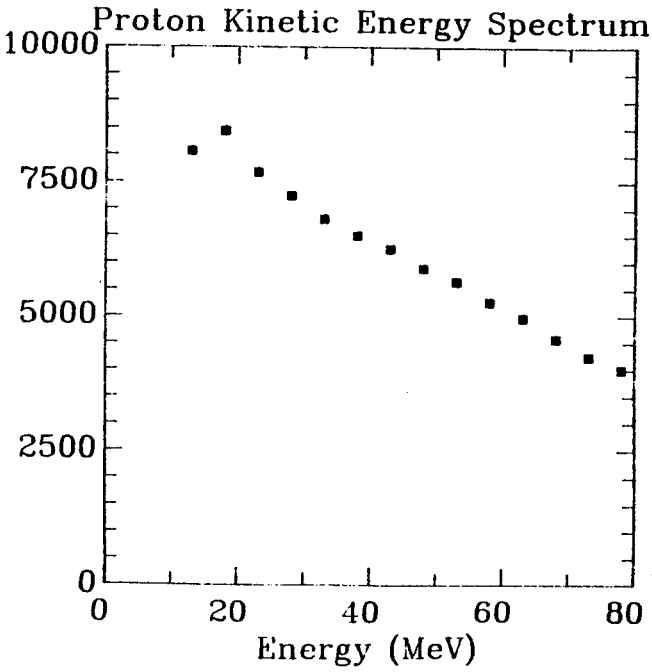

Fig. 2. Proton kinetic energy spectrum, 500 MeV p + Ag. The detector array spans angles from 55° to 75 °.

be generated and compared to a spectrum of randomly generated events to eliminate any structures in the two particle correlations that are a function of the geometry of the detector and its efficiency. From these correlation functions we expect to be able to extract source sizes of the emitting system. The size of the emitting source will be determined by means of a correlation between two particles that are not associated with the decay of a higher lying unstable resonance (deuteron-deuteron for example). One gets a source size that is too small if one uses a pair of particles that are associated with a higher lying state because a large fractions of those coincidence events come from the decay of that state. For those events, the source size is the size of the parent state and not the size of the thermal source from which the original distribution was emitted.

Having determined the size of the thermal source, one can subtract out the portion of the two particle correlation that can be accounted for by emission of two light fragments directly from the source. The portion of the correlation function that is left must come from light particles produced in the decay of excited states in the nucleus that is composed of the two particles. By a determination of the ratios of the peaks in the relative momentum spectra, and matching these peaks with excited states of the composite isotopes, one can determine the temperature of the thermal source as was done in references 5,6,7 and 8. This analysis is underway at the present time.

---

a. Tri-University Meson Facility, Vancouver, British Columbia
b. Simon Frasier University, Burnaby, British Columbia
c. University of Michigan, Ann Arbor, Michigan

References

1. G.D. Westfall et al., Phys. Rev. Lett. 37, 1202 (1976)
2. J. Gosset et al., Phys. Rev. C18, 844 (1978)
3. B.V. Jacak et al., Phys. Rev. Lett. 51, 1846 (1983)
4. D.J. Morrissey et al., Phys. Lett. 148B, 423 (1984)
5. J. Pochodzalla et al., Phys. Rev. Lett. 161B, 275 (1985)
6. C.B. Chitwood et al., Phys. Rev. Lett. 172B, 27 (1986)
7. C. Bloch et al., in print
8. D. Fox et al., submitted for publication

D.A. Cebra, D. Fox, J. Karn, C. Parks, E. Norbeck[a],
G.D. Westfall, W.K. Wilson, J. van der Plicht

The study of nucleus-nucleus collisions at energies near the fermi energy is of interest because of the change in the dominant reaction mechanism as the beam energy is increased. At energies below the fermi energy, the reaction between two nuclei tends to form a highly excited compound nucleus, while above the fermi energy one sees formation of a fireball. The range of energies near this boundary covers a region in which there is a fundamental change in the reaction mechanism. For a symmetric system, the onset of production of an unbound system occurs near 30 MeV/nucleon. At this energy, symmetric nuclei colliding in an inelastic central collision will have just enough internal kinetic energy to completely unbind all of the nucleons in the system leaving free nucleons with no kinetic energy in the center of mass of the system.[1] In general this process does not occur, instead a fraction of the nucleons are emitted with a Boltzmann distribution of kinetic energies, while the remainder forms a residual system.[2]

In this experiment, we studied the manifestations of this change in reaction mechanism near the fermi energy. Observables that we expect to be of interest are the multiplicities of charged particles and the flow angle of matter in an intermediate energy nucleus-nucleus collision. In order to understand the reaction mechanisms that dominate nuclear interactions in this energy regime, one must be able to accurately determine the positions and energies of the light particles that are emitted from the system as it cools and reequilibrates following the reaction. It is also necessary to detect the residual target and projectile fragments to determine the energy transferred during the collision. The detection scheme that we used for this experiment allowed us to detect light, intermediate, and heavy charged particles (see fig. 1). For the detection of highly ionizing fragments (heavy target fragments), we used an array of six parallel plate avalanche counters (PPACs). These detectors covered an angular range from 120° to -120°. The scattering angle of the residual target fragment is a very good indicator of the centrality of the collision.

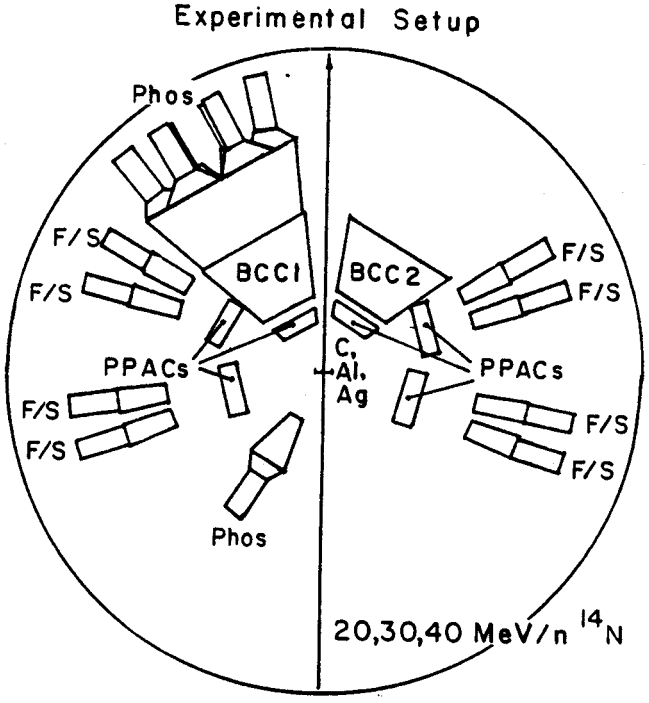

Fig. 1. Diagram of the experimental setup for the part of the experiment that was studying 20, 30, 40 MeV/n ^{14}N + C, Al, Ag. BCC refers to the bragg curve counters, PPAC refers to the parallel plate avalanche counters, Phos refers to the CaF_2/Fast plastic phoswich, and F/S refers to the Fast/Slow plastic phoswichs. Not included on the diagram is the out-of-plane array of seven CaF_2/Fast plastic phoswichs.

For detection of the intermediate mass fragments (Z=10 to Z=25), we used two bragg curve counters (BCCs). Since the BCCs are most sensitive to particles with charge and mass comparible to the beam particles, we set them as far forward as possible. Each covered an

angular range from 10° to 45°. Light particles were detected in several arrays of phoswichs. Over all, the thirty phoswichs covered from 120° to -150° in the plane defined by the PPACs and BCCs, and from 20° to 80° in the plane perpendicular to the reaction plane.

The experimental beams and targets run were 20, 30, 40 MeV/nucleon ^{14}N + C, Al, Ag. These energies and targets covered a range of pairs that spanned the fermi energy boundary. In addition to these energies, we also ran 20 MeV/nucleon ^{86}Kr + Ta and Ag. This beam was the highest energy ever produced at the National Superconducting Cyclotron Laboratory for a total energy of 1.72 GeV. This second part of the experiment was mainly intended to search for reactions in which the target and projectile fused and then broke into several intermediate mass fragments. The chamber setup was modified for this portion of the experiment to move more PPACs to forward angles due to the increased forward focusing with the more energetic beam. Since we were using such a heavy beam, a much larger fraction of the particles emitted by the system will have come from the projectile.

An example of the delta E vs. E maps from one of the phoswich detectors is shown in Fig. 2. The detectors were calibrated with beams of 54 MeV/nucleon deuterons and alphas. The beam was passed through a series of degraders to produce a range of energies in the detectors. We were able to get sufficient control over the output beam from the cyclotron to allow us to run the calibration beams directly into each detector. This allowed us to get an extremely good calibration. The first stage of the analysis will be the determination of the angular distributions of light particles emitted from both the reactions with nitrogen beams and with the krypton beam.

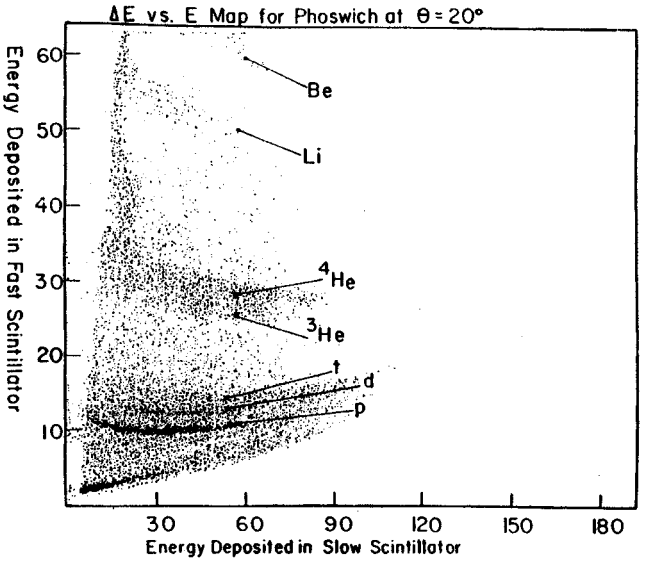

Fig. 2. Delta E vs. E map for a phoswich at 20°.

---

a. University of Iowa, Iowa City, Iowa

References

1. J. Gosset, et al., Phys. Rev. C16, 629 (1977).
2. G. D. Westfall, et al., Phys. Lett. 116B, 118(1982).

PRODUCTION OF UNSTABLE RESONANCES IN 35 MeV/NUCLEON ^{14}N+Ag

D. Fox, D.A. Cebra, C. Parks, R.S. Tickle[a], A. VanderMolen, J. van der Plicht, G.D. Westfall and W.K. Wilson

In the last couple of years a number of experiments have been performed seeking to measure the nuclear temperature through the relative production of excited states of light nuclei. In the first experiments, which studied the production of particle stable states that decay by gamma emission,[1-3] it was shown that the populations of the excited states indicated a temperature much lower than the temperature extracted from the kinetic energy spectra. More recently measurements have been made of particle unstable excited states[4-6]. While these measurements have indicated slightly higher temperatures than the particle stable states, the temperature is still much lower than that extracted from the energy spectra.

We have measured the production of particle unstable light nuclei from 35 MeV/nucleon N+Ag which is the same system studied by Morrissey et. al.[1-3] The measurements were conducted using an array of sixteen fast/slow plastic scintillator telescopes placed behind a three-plane multi-wire proportional counter (MWPC). The plastic scintillators provided energy and particle indentification, while the MWPC provided position information. In a separate run we measured the ground state energy spectra for the He-Be isotopes.

We have carried out detailed efficiency calculations for our setup. The calculations include corrections for reaction losses in the plastic scintillators, the MWPC's response as a function of energy, charge and mass, the individual energy cuts of each telescope, the geometry of the telescopes, and the energy spectra of the bound states. Populations of the observed excited states will be extracted when these calculations are complete.

In addition to measuring the populations of particle unstable resonances, small angle correlations may be used to determine the space-time extent of the emitting system.[4,7,8] Using the calculations of Boal and Shillcock,[8] we have extracted the source radii from the correlations of several particle pairs. The correlation function for two deuterons is shown in Fig. 1 along with calculations for sources of radius 7.0 (solid lines) and 8.0 (dashed lines) fm. The results, shown in Table I, are in general agreement with previous measurements.[4,5]

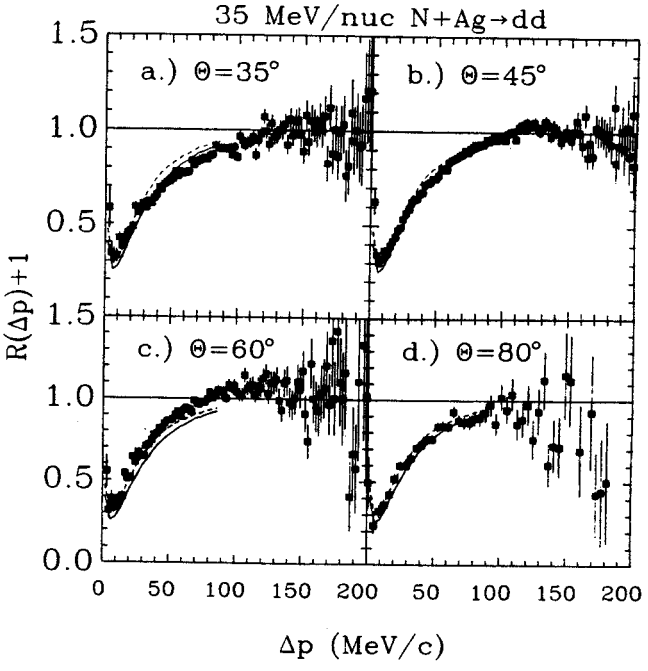

Fig. 1 Two deuteron correlation function for Θ=35°, 45°, 60° and 80°. The solid and dashed lines are calculations for emission from a source of radius 7.0 and 8.0 fm respectively.

Table I
Source Radii

Correlation	Radii (fm)
p+p	4.5±0.3
p+d	9.5±0.4
d+d	7.5±0.4
t+t	6.3±0.5
α+α	4.4±0.3

---

a. University of Michigan, Ann Arbor, Michigan.

References

1. D.J. Morrissey, W. Benenson, E. Kashy, B. Sherrill, A.D. Panagiotou, R.A. Blue, R.M. Ronningen, J. Van der Plicht and H. Utsunomiya, Phys. Lett. 148B,423(1984).
2. D.J. Morrissey, W. Benenson, E. Kashy, C. Bloch, M. Lowe, R.A. Blue, R.M. Ronningen, B. Sherrill, H. Utsunomiya and I. Kelson, Phys. Rev. C32,877(1985).
3. D.J. Morrissey, C. Bloch, W. Benenson, E. Kashy, R.A. Blue, R.M. Ronningen and R. Aryaeinejad, Phys. Rev. C34,761(1986).
4. C.B. Chitwood, C.K. Gelbke, J. Pochodzalla, Z. Chen, D.J. Fields, W.G. Lynch, R. Morse, M.B. Tsang, D.H. Boal and J.C. Shillcock, Phys. Lett. 172B,27(1986).
5. J. Pochodzalla, C.K. Gelbke, W.G. Lynch, M. Maier, D. Ardouin, H. Delagrange, H. Doubre, C. Gregoire, A. Kyanowski, W. Mittig, A. Peghaire, J. Peter, F. Saint-Laurent, B. Zwieglinski, G. Bizard, F. Lefebvres, B. Tamain, J. Quebert, J.P. Viyogi, W.A. Friedman and D.H. Boal, MSUCL preprint #569.
6. C. Bloch, W. Benenson, A.I. Galonsky, E. Kashy, J. Heltsley, L. Heilbronn, M. Lowe, B. Remington, D.J. Morrissey and J. Kasagi, MSUCL preprint #592.
7. S.E. Koonin, Phys. Lett. 70B,43(1977).
8. D.H. Boal and J.C. Shillcock, Phys. Rev. C33,549(1986); D.H. Boal private communication.

LARGE ANGLE CORRELATIONS IN ^{12}C-INDUCED REACTIONS AT 40 AND 50 MeV/NUCLEON

D. Fox, D.A. Cebra, J. Karn, C. Parks, G.D. Westfall and W.K. Wilson

The degree to which thermalization occurs in nucleus-nucleus collisions has been studied for some time.[1-3] Both light particle and complex fragment inclusive energy spectra are thermal in appearance and come from an apparently thermalized source with a velocity intermediate between the projectile and target velocities.[3] Large angle correlations have been used to probe further the question of thermalization in nucleus-nucleus collisions. At 85[4] and 800[5-7] MeV/nucleon the relative importance of direct versus thermal phenomena has been studied by measuring the ratio of in- to out-of-plane correlations. For C+C it was shown that the correlations peak at the energies and angles corresponding to quasielastic nucleon-nucleon scattering. For a large system, C+Pb, the ratio was found to be nearly independent of angle indicating that the system was thermalized. At lower energies, 19-25 MeV/nucleon,[8-10] light systems have been found to be dominated by momentum conservation effects, while heavier systems have been shown to emit preferentially in a plane.

We have shown that light particles seem to be emitted from three thermalized sources. The three sources have projectile-like, target-like and intermediate velocities. We have found no evidence of direct nucleon-nucleon scattering contributions.

The experiment was conducted at the National Superconducting Cyclotron Laboratory using beams of 40 and 50 MeV/nucleon ^{12}C from the K500 Superconducting Cyclotron. The targets were 26 mg/cm^2 graphite, 4.0 mg/cm^2 Ag, and 5.5 mg/cm^2 Au. Particles were detected in twelve fast-slow plastic phoswich telescopes consisting of a 1.6 mm thick fast plastic (BC 412) ΔE detector and a 127 mm long slow plastic (BC 444) E detector. Two of the telescopes were placed in plane with Φ=180° and θ=25° and 45°. An additional two telescopes were placed out of plane with Φ=90° and θ=25° and 45°. The remaining eight telescopes were placed in plane with Φ=0° and θ=15°, 25°, 45°, 55°, 70°, 85°, 100°, and 150°.

The inclusive energy spectra are smooth and decrease monotonically with increasing angle. They show signs of emission from three distinct sources, target-like, projectile-like and intermediate velocity.

Examples of the in-plane two particle correlation functions are shown in Figs. 1 and 2 for d-d and d-^{4}He. The correlations are shown in terms of the two particle correlation cross section, σ_{12}, divided by the singles cross sections, σ_1 and σ_2. In each case one of the particles is detected at θ=-45° and the second particle is detected between θ=-170° and +170°.

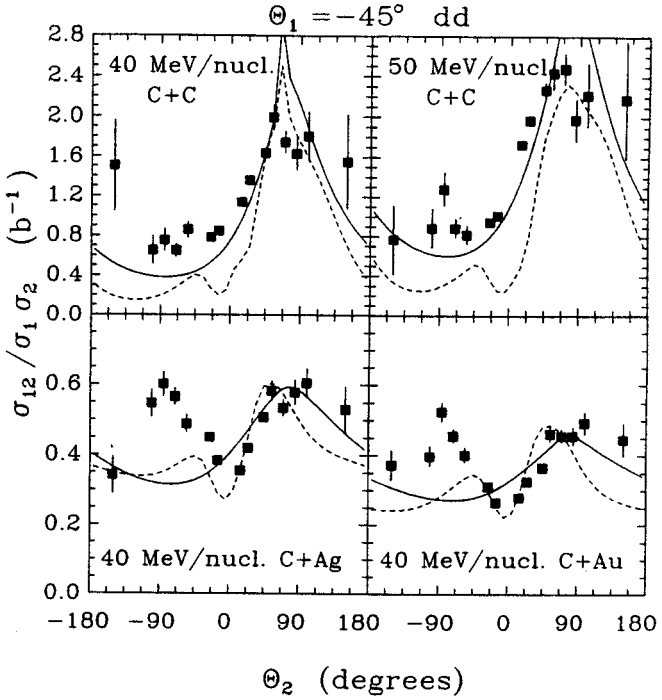

Fig. 1 Two deuteron correlation function where one deuteron is detected at θ=-45°. The lines are the results of momentum conservation calculations that are described in the text.

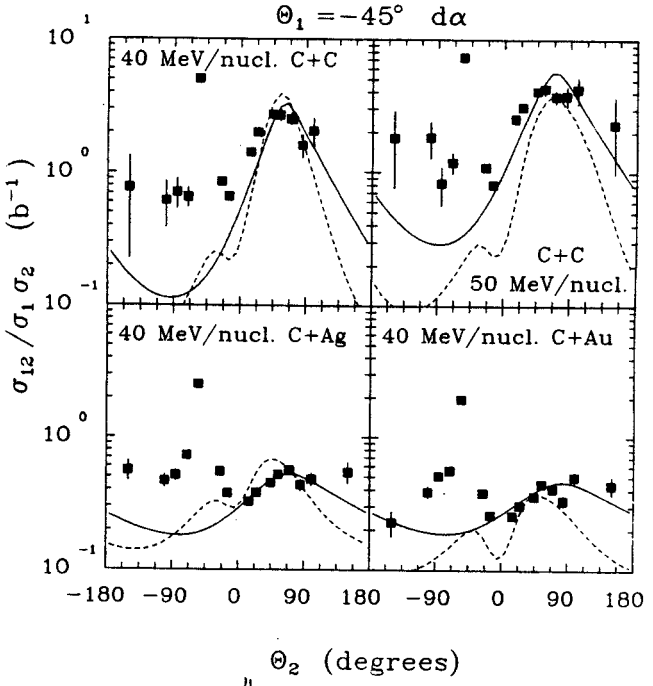

Fig. 2 Deuteron-^{4}He correlation function where the ^{4}He is detected at θ=-45°. The lines are the results of momentum conservation calculations that are described in the text.

A negative angle for the second particle means the two particles were observed on the same side of the beam, while a positive angle indicates emission on opposite sides of the beam. For the d-^{4}He, the case where the ^{4}He was detected at θ=-45° is shown.

In general the correlations for the C+C systems show a broad maximum at positive angles indicating a preference for emission on opposite sides of the beam. The magnitude of the peak increases as the mass of the observed particles increase. For negative angles, the general trend is that the correlations do not change much with angle. The d-^{4}He correlations have a peak at θ=-55°, which comes from the decay of particle unstable states in ^{6}Li. The C+Ag and C+Au systems have different systematic behavior. The correlation function is in general almost symmetric about θ=0° with the same side being only slightly preferred. As in the C+C systems, a peak is observed in the d-^{4}He correlations at θ=-55°. The particle pairs that are not shown all exhibit the same characteristics that are seen in Figs. 1 and 2. The p-p, p-t, p-^{4}He, t-^{4}He, and ^{4}He-^{4}He correlations all have peaks at θ=-55° coming from the decay of particle unstable states.

Energy and momentum conservation effects have been used to explain the observed correlations for small systems at lower energies.[9,10] In order to explore the extent to which our data is effected by conservation laws, we have carried out calculations incorporating these effects. The results of the momentum conservation calculations are shown in Figs. 1 and 2 as solid lines. The calculations have been renormalized to the data at θ=+45° and +55°. The calculations do a good job of reproducing the general trends in the data, but miss some of the details. In the lighter systems the same side correlations are basically flat, except for those cases that have contributions from the decay of resonances, while the calculation predicts a broad minimum at about θ=-80°. The heavier systems have a "V" shaped dip around θ=0°, but the calculations show no such dip.

To study the effect of the other sources, the projectile-like and the target-like, on the two particle correlations we have carried out the momentum conservation calculations explained above for each of these sources. When we add the three sources together we get the dashed lines in Figs. 1 and 2. These calculations take into account only correlations between two particles coming from the same source. Unlike the single source calculation discussed earlier, no normalization has been applied to the three source calculation. The calculation now produces a "V" shape for small θ for the heavier systems that has been previously explained in terms of a rotating ideal gas.[10] Also where the single source calculation had a broad maximum for same side correlations, the three source calculation shows a maximum at about θ=-55°. This maximum is almost as large as the opposite

side maximum for the heavier systems. The most notable disagreement between the data and the three source calculation is the under predicting of the coincident cross section for large θ. This disagreement is probably due to correlations where the particles come from different sources.

Figure 3 shows the ratio of in-plane to out-of-plane correlations for 40 MeV/nucleon C + C, Ac + Au. The solid and dashed lines are the results of momentum conservation calculations described above. The ratio is plotted as a

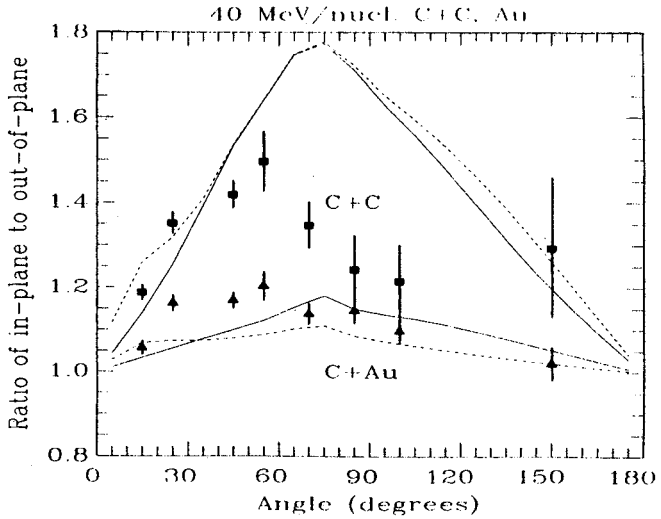

Fig. 3 Ratio of in-plane to out-of- plane correlations for two protons. One of the protons is detected at θ=45° with either φ=180° (in-plane correlation) or with φ=90° (out-of-plane correlation). The lines are the results of momentum conservation calculations that are described in the text.

function of the polar angle θ of the proton detected at φ=0°. The other proton is detected at either (θ,φ)=(45°,180°), an in-plane correlation, or (θ,φ)=(45°,90°), an out-of-plane correlation. The three source momentum conservation calculation reproduces the relative flatness of the data for the C+Au case. For the C+C system the disagreement at large angles between the data and the calculation is probably due to correlations between protons where one proton comes from the target-like source and the other proton comes from the intermediate source. Correlations between protons from different sources should contribute equally to both the in-plane and the out-of-plane correlations thus reducing the ratio of in- to out-of-plane correlations as is seen in the data.

References

1. T.C. Awes, S. Saini, G. Poggi, C.K. Gelbke, D. Cha, R. Legrain, and G.D. Westfall, Phys. Rev. C25,2361(1982).
2. G.D. Westfall, B.V. Jacak, N. Anantaraman, M.V. Curtin, G.M. Crawley, C.K. Gelbke, B. Hasselquist, W.G. Lynch, D.K. Scott, M.B. Tsang, M.J. Murphy, T.J.M. Symons, R. Legrain, and T.J. Majors, Phys. Lett. 116B,118(1982).
3. B.V. Jacak, G.D. Westfall, C.K. Gelbke, L.H. Harwood, W.G. Lynch, D.K. Scott, H. Stöcker, M.B. Tsang, and T.J.M. Symons, Phys. Rev. Lett. 51,1846(1983).
4. P. Kristiansson, L. Carlen, H.-A. Gustafsson, B. Jakobsson, A. Oskarsson, H. Ryde, J.P. Bondorf, O.-B. Nielsen, G. Lovhoiden, T.-F. Thorsteinsen, D. Heuer and H. Nifenecker, Phys. Lett. 155B,31(1985).
5. S. Nagamiya, L. Anderson, W. Bruckner, O. Chamberlain, M.-C. Lemaire, S. Schnetzer, G. Shapiro, H. Steiner and I. Tanihata, Phys. Lett. 81B,147(1979).
6. I. Tanihata, M.-C. Lemaire, S. Nagamiya and S. Schnetzer, Phys. Lett. 97B,363(1980).
7. I. Tanihata, S. Nagamiya, S. Schnetzer and H. Steiner, Phys. Lett. 100B,121(1981).
8. W.G. Lynch, L.W. Richardson, M.B. Tsang, R.E. Ellis, C.K. Gelbke and R.E. Warner, Phys. Lett. 108B,274(1982).
9. M.B. Tsang, W.G. Lynch, C.B. Chitwood, D. Fields, D.R. Klesch, C.K. Gelbke, G.R. Young, T.C. Awes, R.L. Ferguson, F.E. Obenshain, F. Plasil and R.L. Robinson, Phys. Lett. 148B,265(1984).
10. C.B. Chitwood, D.J. Fields, C.K. Gelbke, D.R. Klesch, W.G. Lynch, M.B. Tsang, T.C. Awes, R.L. Ferguson, F.E. Obenshain, F. Plasil, R.L. Robinson and G.R. Young, Phys. Rev. C34,858(1986).

SPIN ALIGNMENT IN THE REACTION $^{22}Ne + ^{170}Er$ AT 10 MeV/A

R. Aryaeinejad, D.J. Morrissey, R. Blue, R. Ronningen
M. Kaplan[a], C. Knott[a], H. Takai[a], J.X. Saladin[a], D. Winchell[a], and I.Y. Lee[b]

The angular momentum transfer and spin alignment of fragments in deep-inelastic heavy ion collisions have been recently investigated by the multiplicity and anisotropy of γ-rays emission from excited fragments[1,2]. Previous measurements have been made with low resolution continuum spectroscopy and, in a few cases, with high resolution discrete γ-ray spectroscopy of one of the fragments. These previous studies have measured the alignment of one fragment as a function of Q-value but have not been able to correlate the spins of the reaction partners.

We have investigated the simultaneous anisotropies and spin alignments of both the light and the heavy fragment from ^{22}Ne on ^{170}Er at 10 MeV/A. The projectile-like fragments (PLF) were detected in 6 surface barrier telescopes located on a cone about the beam axis at an angle of 30° (lab.). The particle detectors were cooled to -20°C to ensure separation of adjacent isotopes. γ-rays from both light and heavy fragments were detected in an array of 5 Compton-suppressed Ge detectors. Figure 1 shows a typical γ-ray spectrum in coincidence with ^{18}O ejectiles. Transitions in ^{168}Yb, ^{170}Yb and ^{172}Yb are seen up to the previously observed $J^{\pi}=18^{+}$ state. These residual nuclei are from the α transfer reaction with successive neutron evaporation.

The intensities of yrast transitions measured in coincidence with light fragments as a function of θ covering the angular range of 10-80° (lab.) were used to obtain the angular correlations. Here, θ is the angle between the γ-ray counter and the normal to the reaction plane defined by the particle detector and the beam. The kinetic energy of the PLF's was sharply peaked as expected for transfer reactions at this bombarding energy. Some

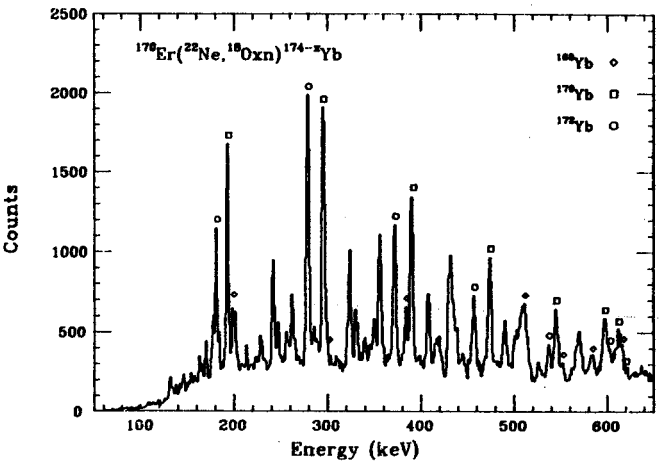

Fig. 1 Spectrum of γ-rays recorded with Ge detectors in coincidence with ^{18}O ejectiles.

representative data and fitted angular distribution functions for both light and heavy fragments are shown in Fig. 2. These angular distributions were used to extract the anisotropy and spin alignment of the fragments using the procedure described by Moretto et al.[3] These results are shown as a function of Z in Fig. 3. No corrections have been made for contributions from the misalignment process of sequential neutron evaporation which proceedes the γ-ray cascade.

For these quasi elastic reactions, the anisotropy of target-like fragment (TLF) γ-rays rises with increasing Z-transfer and peaks at a maximum of ~2.8. The initial rise of anisotropy with increasing Z is due to a rapid buildup of aligned spin by particle transfer at the periphery of the nuclei. The subsequent fall of the anisotropy at larger Z indicates that the relative importance of the aligned component of the transferred angular momentum is decreasing compared to the randomly-oriented thermal components of spin. These random components cause a significant decrease in the alignment. As expected, we have observed larger

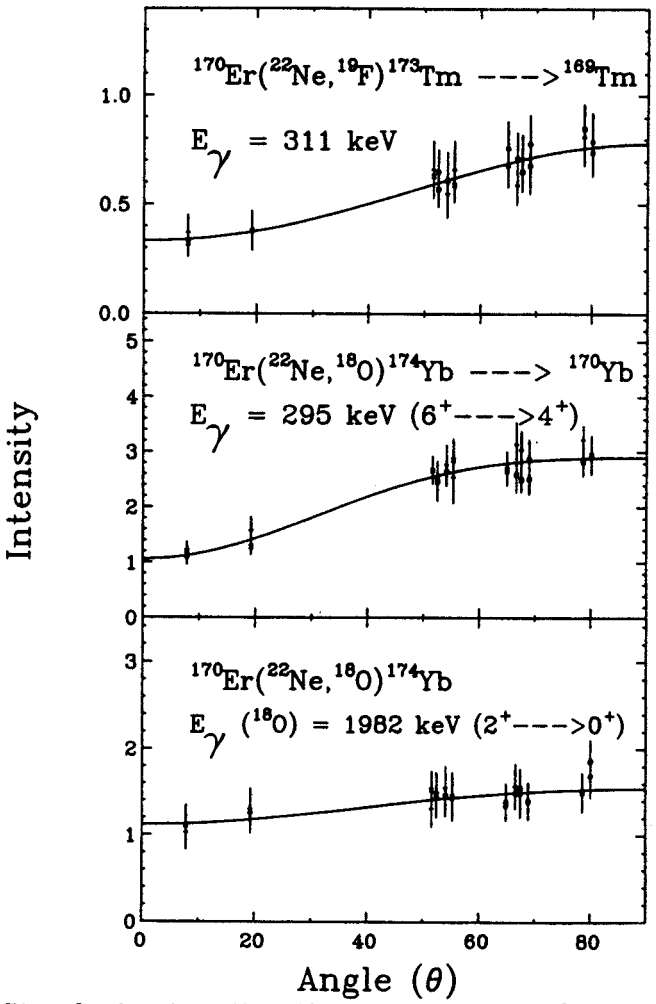

Fig. 2 Angular distributions of γ-rays for both light and heavy fragments in coincidence with ejectiles. The solid curve is Legendre polynomial fit to the data.

anisotropies than those previously seen in the continuum γ-ray spectroscopy. This is due to a substantial admixture of dipole transitions among the quadrupole γ-ray transitions that are not separated by the continuum technique resulting in a smaller anisotropy even if the fragment angular momentums are completely aligned.

The most interesting new feature of the present results is the comparison of the TLF and PLF spin alignments shown in Fig. 3. For example, the spin alignment parameter, P_{zz}, of ^{18}O fragments was found to be 43% whereas the alignment of ^{170}Yb fragments in coincidence with the ^{18}O ejectiles was 70%. Combination of these data with fragment spins will allow us to determine the correlation of the alignments.

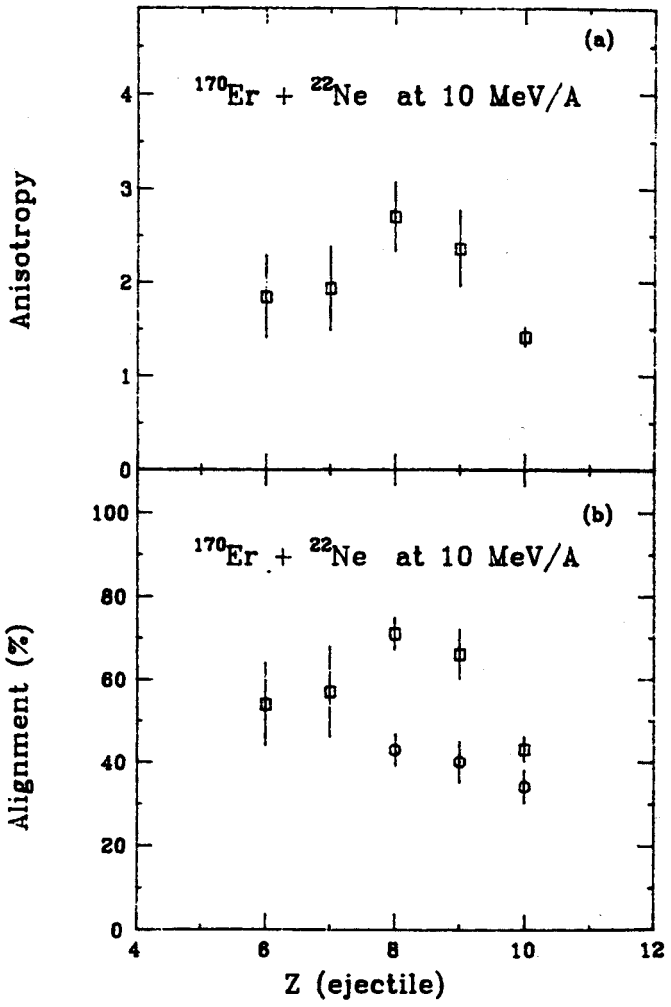

Fig. 3 (a)Anisotropy of the stretched E2 yrast transitions in target-like fragments as a function of Z of ejectiles. (b)Spin alignment in TLF's (squares) and in PLF's (circles) as a function of Z of ejectiles.

a. University of Pittsburgh.
b. Oak Ridge National Laboratory.

References

1. A.J. Pacheco, G.J. Wozniak, R.J. McDonald, R.M. Diamond, C.C. Hsu, L.G. Moretto, D.J. Morrissey, L.G. Sobotka and F.S. Stephens, Nucl. Phys. A397,313(1983).
2. G. Mouchaty, D.R. Haenni, S. Nath, U. Garg, R.P. Schmitt, Z. Phys. A316,285(1984).
3. L.G. Moretto, S.K. Blau and A.J. Pacheco, Nucl. Phys. A346,125(1981).

VERY-HIGH ENERGY ($E \rightarrow E_{BEAM}$) LIGHT PARTICLE PRODUCTION NEAR 0° IN HEAVY-ION COLLISIONS, E/A ≤ 40 MeV/U

F.D. Becchetti,[a] J. Jänecke,[a] S. Shaheen,[a] R. Stern,[a] A. Nadasen,[b] and D. Kovar[c]

Alpha particles with energies approaching the full beam energy, and protons, deuterons and tritons with a significant fraction of the beam energy (~one-half) have been observed in heavy-ion collisions near $\theta = 0°$ for projectiles $Z > 8$ with $E/A \approx 10$ to 40 MeV/u stopped in thick targets. Fits to the spectra assuming only projectile fragmentation with Fermi motion in the projectile require rather large source temperatures (T_s ~10 to 50 MeV). Alternate processes, such as cluster transfer mechanisms are suggested.

Studies[1-4] of heavy-ion collisions at E/A ~10 MeV/u to 20 MeV/u have indicated the importance of non-equilibrium processes in the emission of energetic light particles. The production of nucleons and other particles at forward angles with velocities several times that of the projectile have been observed by many groups and is usually attributed to projectile fragmentation with Fermi motion of the light particle,[2,3] described by a source temperature T_s, accounting for the additional velocity component. However, experiments reported by Borcea et al.[5] and those done[6,7] at the Hahn-Meitner Institute (VIKSI) have suggested that high-energy alpha particles observed near $\theta = 0°$ in Ne-induced collisions, $E/A < 20$ MeV/u, may arise from other mechanisms such as cluster transfer reactions. Since the latter, e.g. (^{20}Ne,α) as an ^{16}O transfer, have a small Q-value, they can produce light particles approaching the full beam energy particularly near $\theta=0°$. Thus heavy projectiles with E/A of tens of MeV/u may produce ~GeV light particles. We have studied this phenomenon with a variety of projectiles ($Z > 8$), $E/A \approx 9$ to 40 MeV/u, at the MSU NSCL and ANL ATLAS facilities.

The small angle data were primarily taken using a 50 mm diameter by 150 mm long BGO scintillator situated about 0.5 m behind a thin tantalum target which also served as a beam stop and permitted measurements at $\theta = 0°$. Additional detectors, usually 50 mm diameter by 100 mm NaI(Tℓ) or 100 mm x 100 mm NaI(Tℓ) were situated at angles $\theta > 0°$. The BGO detector could stop protons up to about 400 MeV and α particles up to 1.5 GeV, although the efficiency for protons is somewhat less than unity above 200 MeV. The NaI(/tℓ) detectors could stop protons of about 150 MeV and α particles of about 600 MeV.

Particles were identified[8] in the BGO using time-of-flight (TOF) while those in the NaI(Tℓ) were identified with pulse-shape discrimination (PSD). A PSD signal of $Z = 1$ vs. $Z = 2$ was observed for BGO and was used to verify the TOF identification. Likewise, TOF in the NaI detectors was used as an alternate particle identification parameter. The detectors were calibrated at the Indiana University Cyclotron Facility (IUCF) using 150 MeV protons and 270 MeV ^{3}He ions.

The projectiles and bombarding energies studied are shown in Table I and were obtained from the Argonne National Laboratory (ANL) ATLAS linac or the NSCL superconducting cyclotron, which were both tuned i.e. phase selected for TOF measurements with $\Delta t_{beam} \leq 1$ nsec.

Some of the light particle spectra observed at $\theta = 0°$ from the NSCL experiments are displayed in Figure 1. They typically peak at an energy near that corresponding to the projectile velocity (although some spectra are cutoff by lower discriminators) and then fall off as ~exp $-E_L/T_L$ where E_L is the fragment's

Table I

System	$E^{(b)}$ (MeV)	E/A MeV/u	Protons T_L (MeV)[a]	Protons T_S (MeV)[b]	Alphas T_L (MeV)[a]	Alphas T_S (MeV)[b]
$^{32}S + ^{181}Ta$[c]	305	9.5	16	11	32	18
	450	14	24	16	48	26
$^{58}Ni + ^{181}Ta$[c]	600	10.3	8	6.5	18	13
$^{16}O + ^{181}Ta$[d]	480	30	14	9	30	17
	640	40	20	13	40	24

Footnotes to Table I

a) $\frac{dN}{dE} \approx e^{-E_L/T_L}$

b) Fragmentation-model fit, viz. moving source with projectile (beam) velocity and source temperature, T_S. T_S is adjusted to fit the observed spectra at $\theta = 0°$. We assume that most high energy particles come from the high-energy portion of the (stopped) beam.

c) Data from ANL ATLAS experiments

d) Data from MSU NSCL experiments

lab energy and T_L is the slope parameter. Except for the ^{58}Ni projectiles (Table I), the α spectra near $\theta = 0°$ extend out to nearly the full beam energy while the proton spectra extend out to about half the beam energy. Deuterons, tritons and ^3He particles are much less intense but also extend out to a significant fraction of the beam energy. As observed[5-7] in Ne-induced reactions at E/A ≈ 10 MeV/u, near $\theta=0°$, alpha particles are emitted several times more copiously than protons. Also, as observed by others, the high-energy portions of the light particle spectra, especially for alpha particles, are peaked at an angle near $\theta=0°$, whereas the lower-energy particles are emitted more isotropically.[1-4] The observed slope parameters, T_L and deduced source temperatures, T_S, are displayed in Table I.

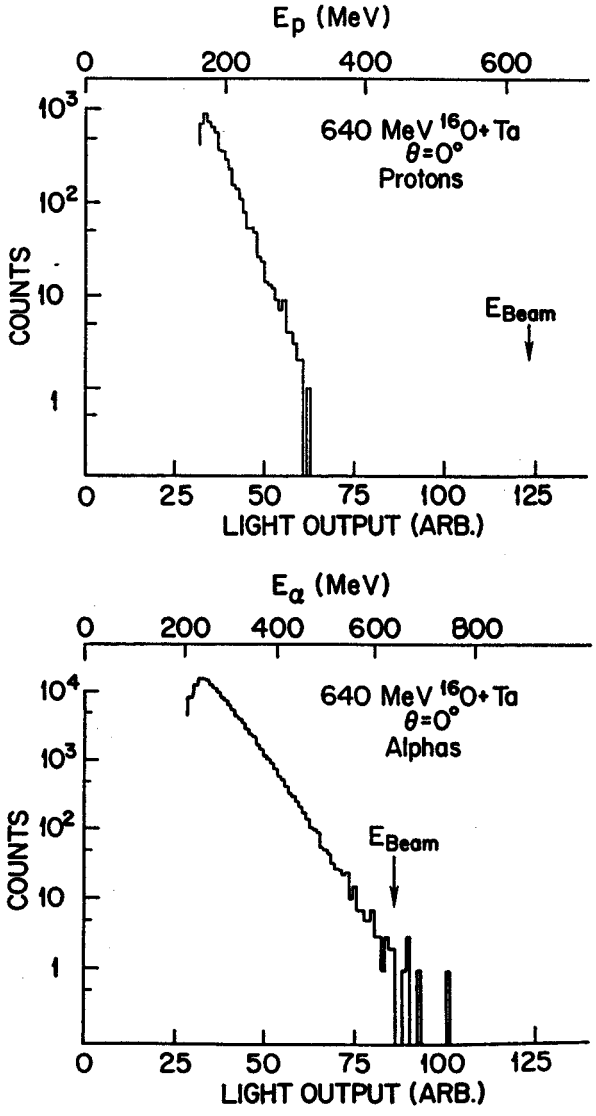

Fig. 1. Proton (top) and alpha particle (bottom) spectra observed at $\theta = 0°$ for 40 MeV/u ^{16}O ions stopped in a thin Ta foil.

We have calculated the spectral shapes expected[2] assuming fragmentation of a source moving with the projectile velocity with Fermi motion corresponding to a source temperature, T_S, i.e. projectile fragmentation. The source temperature T_S for emitted nucleons should be comparable to a typical nuclear Fermi energy, T_F, of 3 to 8 MeV. Instead, we often require source temperatures of 8 to 24 MeV to reproduce the proton spectra, and 13 to 48 MeV to reproduce the alpha spectra.

As suggested by (Ne,α) experiments at lower energies, the high-energy portions of the alpha spectra, which exhibit $T_s > 30$ MeV, and the fact that $E_L^{MAX} \approx E_{Projectile}$ suggest that mechanisms other than fragmentation e.g. cluster transfer may be important and as a source of very-high energy light particles. We are presently extending our measurements at MSU NSCL to heavier projectiles ($A \geq 40$, $E/A \geq 20$ MeV/u) including thin target measurements at $\theta = 0°$ utilizing a double-foil/TOF technique we have recently developed.

---

a. University of Michigan, Ann Arbor, MI
b. University of Michigan-Dearborn, Dearborn, MI
c. Argonne National Lab, Argonne, IL

References

1. H.C. Britt and A.R. Quinton, Phys. Rev. 124, 877 (1961)
2. C.K. Gelbke, et al., Phys. Lett. 70B, 415 (1977)
3. R.L. Auble, et al., Phys. Rev. C25, 2504 (1982); Phys. Rev. C28, 1552 (1983)
4. M.N. Namboodiri, et al., Nucl. Phys. A367, 313 (1981)
5. C. Borcea, E. Gierlik, R. Kalpakchieva, Yu.Ts. Oganessian and Yu.E. Penionzhkevich, Nucl. Phys. A351, 312 (1981)
6. Ch. Egelhaaf, G. Bohlen, H. Fuchs, A. Gamp, H. Homeyer and H. Kluge, Phys. Rev. Letters 46, 813 (1981)
7. H. Machner, D. Protic, G. Riepe, H.G. Bohlen, and H. Fuchs, Phys. Rev. C31, 443 (1985)
8. F.D. Becchetti, P.M. Lister and C.E. Thorn, Nucl. Instrum. Meth. 225, 280 (1984)

SUBTHRESHOLD PION PRODUCTION WITH La BEAMS AND A MULTIPLICITY FILTER

J. Miller[a], W. Benenson, J. Bercovitz[a], G. Claesson[a], J.-F. Gilot[b], G. Krebs[a], G. Landaud[c], G. Roche[a], L. Schroeder[a], J. van der Plicht and J. Winfield

Subthreshold pion production with heavy ions has been studied since 1979[1] with the aim of observing collective effects in the hot,dense nuclear matter formed in the interaction zone of the collision. However, only in the lowest energy experiments[2], right near the conservation of energy threshold, have these effects been shown to exist definitively. In general, the experiments on subthreshold pion production have been carried out with light beams, mainly ^{12}C and ^{20}Ne, and without any impact parameter selection.

In the experiment reported here we follow up on a previous work carried out with a heavy system, the La + La reaction at E/A = 246 MeV[3]. In the present work we have added a multiplicity filter, full angular distributions, and data at much lower energies, 138 and 183 MeV. The experiment was carried out at the Lawrence Berkeley Laboratory Bevalac using the beam 30-2 single arm spectrograph[4]. Several modifications to the spectrograph were made for this experiment including an absorber on the focal plane to stop light ions of the same rigidity of the positive pions. The most important modification was the 110 element multiplicity filter array of roughly cylindrical geometry placed just downstream from the target.

The data from this experiment show several interesting features with respect to a) multiplicity selection, b) angular distributions, c) beam energy dependence, and d) Coulomb effects.

a) In Fig. 1 the multiplicity distribution is given for protons and pions at nearly the same angle and kinetic energy. Given that the unbiased multiplicity is peaked at zero, the data seem to show that both the protons and the pions are produced predominantly in central collisions. However the protons have a low multiplicity component at small angles that is almost absent for the pions.

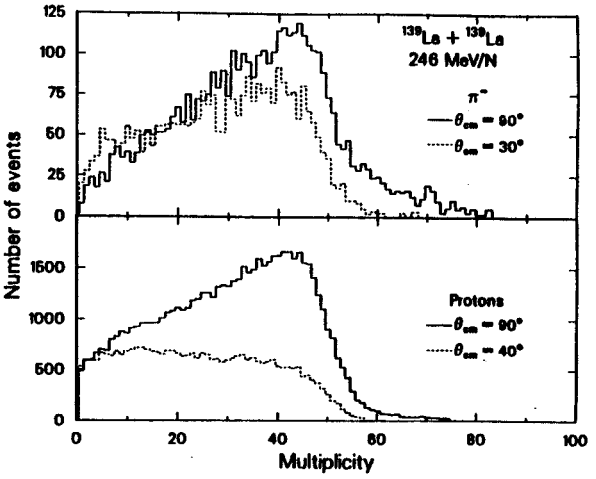

Fig. 1. Number of events vs. associated charged particle multiplicity for protons and negative pions at two different angles in La + La collisions at E/A = 246 MeV.

b) In Fig. 2 the spectra of negative pions is given for a range of angles in the center of mass system. The spectra are exponential and almost independent of angle.

c) The beam energy dependence of the total cross section is quite different for La + La as

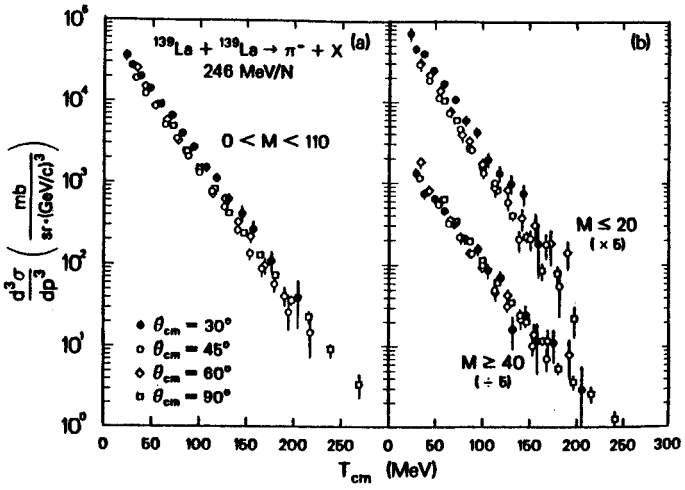

Fig. 2. Spectrum of negative pions at various cm angles for La +La at E/A = 246 MeV.

compared to Ne + NaF. In Fig. 3 the Ne + NaF data has been scaled by $(A_T^{2/3}+A_P^{2/3})$ which usually works very well for sets of data at the same beam energy. However in this case there is a marked deviation which becomes more important the more you go below threshold. This effect is what one would expect for coherent volume production.

d) The cross section for pion production in La + La collisions is almost independent of charge as is seen in Fig. 4. This is in spite of the fact that the neutron excess of the beam and projectile should favor negative pions. The Coulomb shift of the charged pions due to the charge of the source is apparently just enough to cancel the excess of negative pions. About 30% of the total charge is enough to do this. There is also a marked difference between negative and positive pions at the lowest energy. If the process is viewed as statistical[5], then the cross section should be proportional to the true absorption cross section of pions in the appropriate nucleus. This comparison is shown in Fig. 5. The agreement probably indicates the suitability of use of pion capture cross sections as the elementary process in calculations of the pion production.

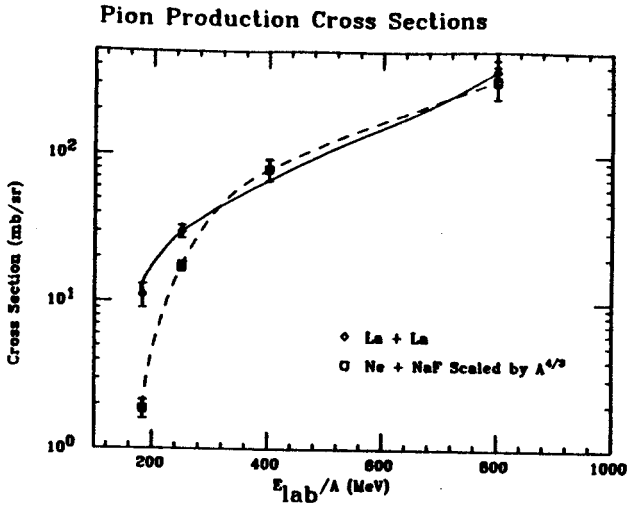

Fig. 3. Total cross section for pion production in La + La and Ne + NaF collisions for various beam energies. The data have been scaled (see text).

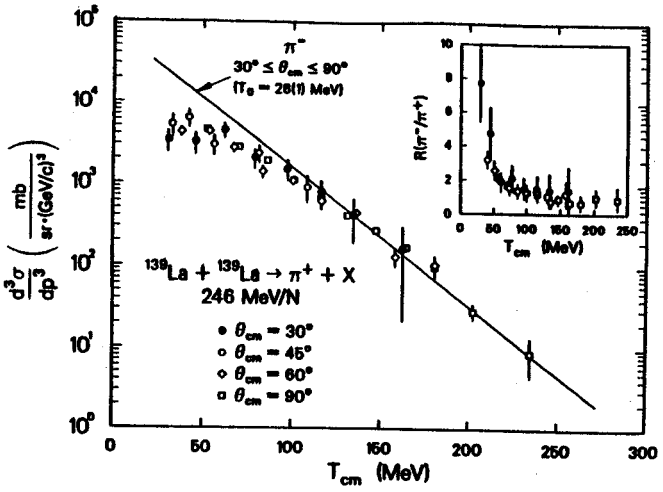

Fig. 4. Comparison of negative and positive pion spectra at 90° cm for La + La at E/A = 246 MeV.

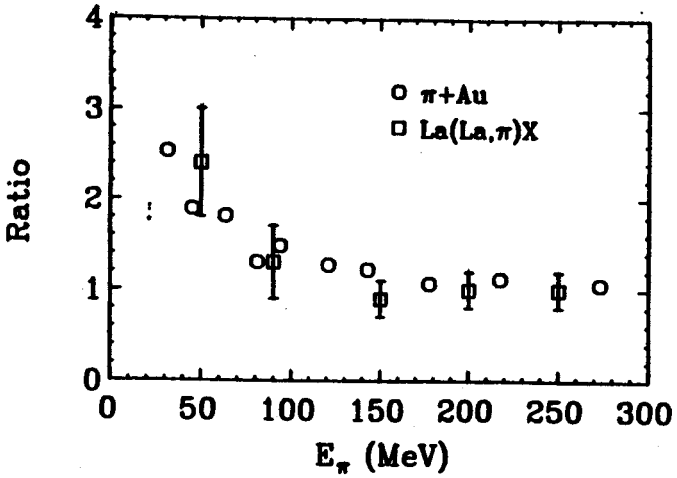

Fig.5. The ratio of negative to positive pion production for E/A = 246 MeV. The curves are the same ratio for negative and positive pion absorption in Au (Nakai et al. Phys. Rev. Letters 44,1446(1980).

---

a. Lawrence Berkeley Laboratory, Berkeley CA.
b. Department of Physics and Astronomy, Louisiana State University
c. Universite de Clermont II-IN2P3, F63170 Aubiere, France

References

1. W. Benenson et al., Phys. Rev. Letters 43,683(1979)
2. J. Stachel et al., Phys. Rev. C33,1420(1986)
3. G.F. Krebs et al., Phys. Letters B171,37(1986)
4. S. Nagamiya et al., Phys. Rev. C24,971(1981)
5. A. Bonasera and G. Bertsch, to be published

STREAMER CHAMBER STUDY OF NEAR-CENTRAL COLLISIONS WITH CCD CAMERAS

S.P. Angius, G.M. Crawley, C. Djalali, D. Fox, M. Maier, R.S. Tickle[a], and G. Westfall

An experiment was carried out at the LBL streamer chamber, in which the CCD camera system developed at MSU was used to record near-central collisions of Nb on Nb at 100 and 200 MeV/nucleon. Over 1000 good events were collected at each energy.

The use of CCD cameras eliminates the need for handling and developing film, and the digitized images are directly stored on magnetic tape during the data-acquisition. Such images easily lend themselves to digital image-enhancement, which makes the tracks more visible and eliminates unwanted features such as flares and background illumination. Using the image-enhanced pictures, a track-recognition program attempts to find and follow all the tracks in the event. Any omissions or errors can be later corrected by an operator. The extent of this intervention is strongly multiplicity-dependent (the higher the number of tracks, the higher the likelihood of crossing and partially overlapping tracks), and it also depends on the overall quality of the image. For the 100 MeV/nucleon data, with an average multiplicity of about 30 charged particles, the manual intervention is reduced to about 10 to 15 minutes per view. In comparison, a completely manual scanning of photographic film takes about 1 minute per track, at best.

After a third-degree polynomial has been fitted to the tracks, and all three views of an event have been processed, the Three View Geometry Program (TVGP) reconstructs the trajectory of each fragment in three-dimensional space, determining radius of curvature (R), emission angles (dip and azimuthal), and length of the track. Since the magnetic field B is known, R gives the magnetic rigidity of a particle, RB=p/Z, where p is the total momentum and Z the charge. Therefore, identification of Z is necessary to determine the momentum of a fragment.

Particle identification, in a streamer chamber, relies on the determination of the track intensity. But, while the energy loss of a particle in a gas is proportional to Z^2, the intensity of the light emitted during the formation of streamers does not show the same charge dependence. Work on the intensity analysis is in progress, and several problems are being investigated. The first is the proper algorithm for mass identification. The event-to-event intensity normalization also appears to be a critical factor in the analysis. In Fig. 1 the track intensity, as a function of position along the track, is plotted for a proton stopping in the chamber. The curve shows the Bragg peak typically observed for stopping particles.

At the present stage, 300 events at 200 MeV/nucleon, and 170 at 100 MeV/nucleon have been analysed through the track-recognition program, and for about 50 of them rigidities and emission angles have been calculated.

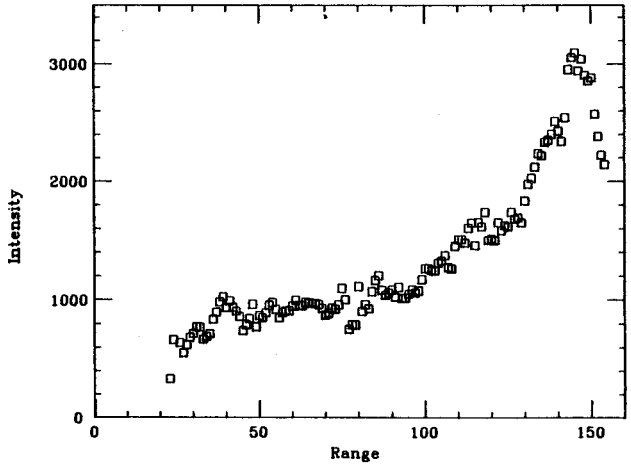

Fig. 1. Bragg peak observed for a proton stopping in the gas of the streamer chamber.

The first piece of information that can be extracted from the analysis is the average charged-particle multiplicity. Histograms of such multiplicities are plotted in Fig. 1 and 2 for the 100 and 200 MeV/nucleon data, respectively. The curves are obtained by fitting a Poisson distribution to the experimental points. The centroids of the distributions (mean charged-particle multiplicity) are 34.4 at 100 MeV/nucleon and 46.8 at 200 MeV/nucleon.

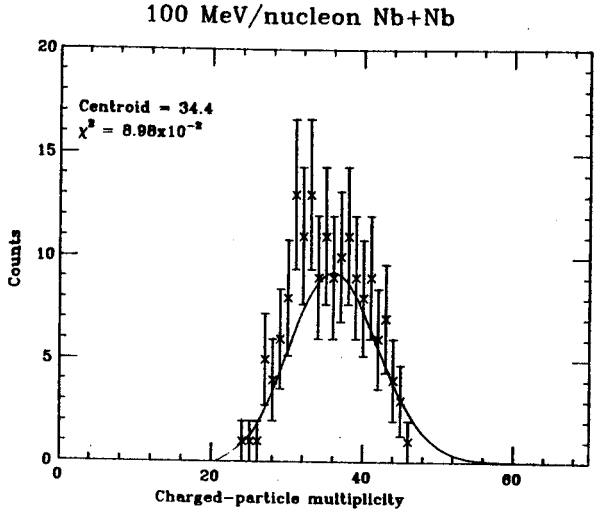

Fig. 2. Multiplicity distribution for 170 events at 100 MeV/nucleon. The curve is obtained by fitting the experimental points with a Poisson distribution.

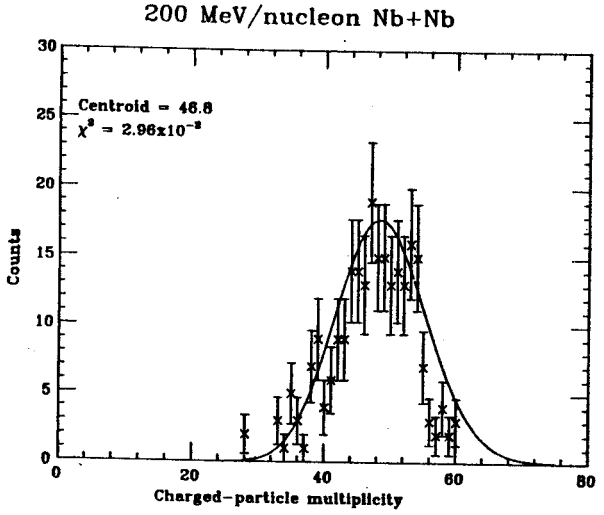

Fig. 3. Multiplicity distribution for 300 events at 200 MeV/nucleon. The fit with a Poisson distribution gives a mean charged-particle multiplicity of about 37.

One of the purposes of this experiment is to study sidewards collective flow, using the transverse momentum analysis technique proposed by Danielewicz and Odyniec[1]. Ideally, momentum, charge and mass of all fragments emitted in a collision should be known, in order to perform this type of analysis. Presently, only rigidities and an approximate estimate of the intensity are know for our data. From this, assumptions can be made about the fragment mass and, by testing momentum, energy, and charge conservation for each event, A and Z can be estimated for all particles. A computer code[2] has already been adapted to the analysis of streamer chamber events, and has been tested, with encouraging results.

---

a. University of Michigan, Ann Arbor, MI.

References

1. P. Danielewicz and G. Odyniec, Phys. Lett. 157B,146(1985).
2. L. Csernai, Private Communication.

NEUTRON DECAY OF EXCITED NUCLEAR STATES IN HEAVY ION COLLISIONS

C. Bloch, W. Benenson, A.I. Galonsky, E. Kashy, J. Heltsley, L. Heilbronn, M. Lowe, B. Remington[a], D.J. Morrissey, and J. Kasagi[b]

Recently, a new type of temperature measurement has been developed and employed for studies of nuclear collisions[1]. By assuming that the populations of the states of an isotope emitted from a nuclear reaction are given by a Boltzmann distribution, one can obtain a temperature by measuring the ratio, R, of two populations. This ratio is related to the temperature, kT, in the following way:

$$R = \frac{(2j_1+1)}{(2j_0+1)} \times \exp(\frac{-\Delta E}{kT}), \qquad (1)$$

where j_0 and j_1 are the spins of the two states, and ΔE is the energy difference between the states. Temperature measurements of this type can be divided into two categories: those that measure bound state populations and those that measure unbound state populations. This distinction seems to be important since measurements of the populations of unbound states in light nuclei systematically yield temperatures around 4 or 5 MeV[2,3] while those of bound states yield temperatures from 0.5 to 1 MeV[1,4,5] for intermediate-energy (E/A=20 to 60 MeV) heavy-ion reactions. Attempts to reconcile these differences have centered on preferential feeding of the ground state by sequential decay as discussed in Refs. 4 and 6. The bound state populations will, of course, fail to reflect the initial Boltzmann distribution if there is significant differential feeding of any of the observed states from particle unbound states in larger nuclei. This effect is expected to be greatest for those ratios which involve the ground state population. As part of a larger experiment[7], we have measured the extent of feeding from sequential decay for two systems previously used in bound state temperature measurements.

A beam of 490 MeV $^{14}N^{5+}$ ions was provided by the K500 cyclotron. The target was a self-supporting foil of natural silver, 1.8 mg/cm^2 thick. Particle inclusive spectra were obtained from four silicon ΔE-E telescopes each with 300 mm^2 area. The ΔE detectors were either 50 μm or 100 μm thick, while the E detectors were each 1000 μm thick. As in Ref. 8, coincident neutrons were detected in ten liquid scintillators (NE213) placed at a wide range of angles in the horizontal plane. These neutron detectors were placed at distances from 130 cm to 206 cm from the target. The typical neutron detector had a geometric solid angle of approximately 7.5 msr. Thin (0.6 cm) plastic scintillation paddles were placed in front of the neutron detectors and were used to veto coincidences with charged particles electronically. The in-beam background of scattered neutrons was measured by taking data with shadow bars between the neutron detectors and the target.

The neutron time-of-flight was measured relative to the charged particle signal in the ΔE detectors of the telescopes. Neutrons were distinguished from γ rays by pulse shape discrimination. The neutron detector efficiency as a function of energy was calculated with the code TOTEFF[9] and folded into the neutron data. Using a technique developed by Kiss et al.[10] it was possible to observe the neutron decay of the 2.255 MeV excited state of ^{8}Li and that of the 7.456 MeV excited state of ^{7}Li, which feed the ground states of ^{7}Li and ^{6}Li, respectively. The present results indicate that the feeding is sufficient to increase substantially the previously extracted temperatures.

Figure 1 shows the velocity distribution of the neutrons shifted to the moving frame of the

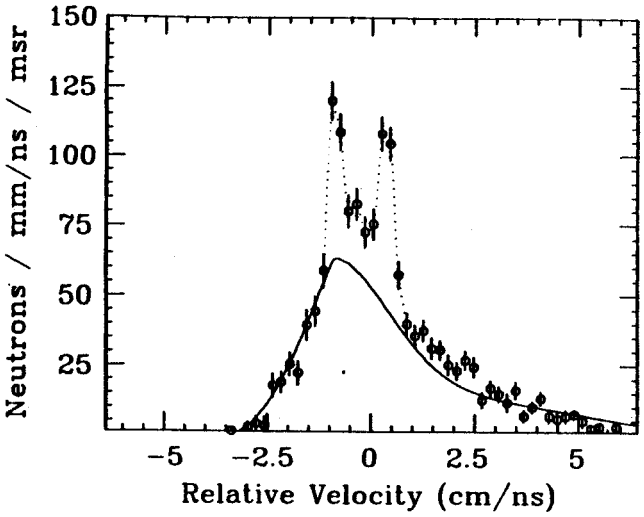

Fig. 1. The yield of neutrons at 50° in coincidence with ^{7}Li at 50° as a function of the relative velocity (neutron velocity minus ^{7}Li velocity). The solid line shows the thermal background (see text), while the dots are to guide the eye.

coincident ^{7}Li on an event-by-event basis. Neutrons from the decay of the 2.255 MeV state in ^{8}Li give rise to a peak at ±0.61 cm/ns in the moving frame of the ^{8}Li. The neutron kinetic energy spectra (determined from the neutron time-of-flight) were fit using a moving source model[11] with two sources. The parameters from the faster source also provided a reasonable fit of the charged particle spectra. Using the parameters from these two energy distributions, it was possible to calculate the relative velocity between uncorrelated charged particles and neutrons. This uncorrelated thermal relative velocity distribution (shown in Fig. 1 as the solid line) was in very good agreement with the data from non-colinear geometries (not shown) and was subtracted from the data points in order to extract the number of ^{8}Li produced in the neutron emitting state.

The geometric efficiency of the neutron detector for observing the decay of this state in ^{8}Li depends on the velocity of the emitting system and the emission velocity of the neutron. This geometric efficiency, $\varepsilon(E)$, was determined by a Monte-Carlo calculation as a function of the ^{8}Li energy both for each of the two peaks seen in Fig. 1. An average geometric efficiency, $\langle\varepsilon\rangle$, was then obtained by the following equation:

$$\langle\varepsilon\rangle = \frac{\int\varepsilon(E)Y(E)dE}{\int Y(E)dE}. \qquad (2)$$

Dividing the number of neutrons observed in each peak by the average efficiency gave the total number of ^{8}Li in the 2.255 MeV state. A similar analysis of neutron emission from the 7.456 MeV state in ^{7}Li was used to determine the number of ^{7}Li in that excited state. The total ^{7}Li yield was corrected for ^{8}Be contamination[5] (about 20% of the observed ^{7}Li yield). In addition, the data were corrected for the fact that this state branches to ^{6}Li+n only 77% of the time[12].

Table I contains the ratio of the two measured unbound excited states of Li to the populations of the ground states and previously measured[4,5] bound excited states and the temperature implied by Eq. (1). The calculated temperature of 3.0(4) MeV (from ^{7}Li (7.456) and ^{7}Li (0.478)) is higher than the 0.54 MeV observed with the bound excited state[5]. This is qualitatively consistent with feeding arguments since the present measurement does not involve

TABLE I. Ratios, R, and their corresponding temperatures, kT, from Eq. (1).

States Compared	R (ratio)	kT (from R and Eq. (1))
^{7}Li(7.456) to ^{7}Li(g.s.)	0.06(2)	2.3(2) MeV
^{7}Li(7.456) to ^{7}Li(0.478)[a]	0.30(9)	3.0(4) MeV
^{8}Li(2.255) to ^{8}Li(g.s.)	0.33(8)	1.6(3) MeV
^{8}Li(2.255) to ^{8}Li(0.9808)[a]	6.2±5.9	≥ 0.6 MeV

[a]Population of γ-emitting states from Refs. 4 and 5.

the ground state and should therefore be less susceptible to the effects of feeding from sequential decay.

Considerable beam time (about 1/3 of the total experiment) was devoted to the shadow bar runs so that their statistical uncertainty would not contribute significantly to the final data. The systematic errors are primarily due to uncertainties in determining the geometrical efficiency for observing the neutron decay. Any misalignment of the neutron detector with respect to the target and the silicon telescope will result in overestimating the geometric efficiency, and hence underestimating the yield from the state in question. However, due to the large target-to-detector distance of 130 cm, it was possible to position the neutron detectors such that their angles were known to ±0.1°, which introduced a relatively insignificant effect on the geometric efficiency. A finite-sized beam spot and possible error in centering the beam have much greater effect on the efficiency. In this experiment, these effects produced the equivalent of a detector misalignment of about 0.6 degrees. The geometric efficiency is quite sensitive to this. For example, a misalignment of 1° reduces $\langle\varepsilon\rangle$ by 1/3, which produces a 50% increase in the calculated populations. The values and uncertainties used for the geometric efficiencies reflect the size and location of the beam spot. The results shown in Table I reflect the systematic uncertainties combined with the statistical errors. The dependence of the temperature given by Eq. (1) on the ratio is very slow in this neighborhood. For instance, increasing the ratio of the populations of the 7.456 MeV state to the 0.478 MeV states in ^{7}Li by 30% only increases the temperature by 13%. To reflect a temperature of 5 MeV, this ratio would have to be 0.743, more than twice as large as observed.

The feeding of the ^{7}Li yield from the 2.255 MeV state in ^{8}Li is defined as the number of ^{8}Li in that state divided by the total number of observed ^{7}Li (corrected for ^{8}Be contamination). The amount of feeding of the ^{7}Li inclusive yield from sequential decay of the 2.255 MeV state in ^{8}Li is 6(2) percent. Similarly, the feeding of the ^{6}Li inclusive yield via neutron emission from the 7.456 MeV state in ^{7}Li is 4(1) percent. These feedings alone will produce only a small correction in the temperatures extracted in Refs. 1, 4, and 5, which still gives temperatures less that 1 MeV. However, these measurements are only from one decay channel. These values plus a model for the sequential decay can be used to estimate the total feeding from all possible decay channels.

An attempt to determine the extent to which feeding from sequential decay reduces the observed fractions reported in Refs. 4 and 5 can be made with the quantum-statistical model of Hahn and Stöcker[6]. For a given temperature (kT), the model assumes an initial statistical equilibrium distribution from infinite nuclear matter based on the binding energy of isotopes, including the excited state populations (using all known states). Subsequently, the final isotope distributions are calculated using all known decays and their branching ratios. The other model parameters were chosen to be appropriate values: the break-up density, ρ, was set at 1/4 of normal nuclear matter density, and the initial proton to neutron ratio, Z/N, was 0.88.

For temperatures above 2 MeV and the other parameters as specified above, the model predicts feeding of around 40% to the ground states of the Li and Be isotopes. The feeding is significant in that the predicted fractions of excited state populations for low-lying particle bound states can be brought close to the observed values[13]. These types of calculations have suggested that feeding may be the solution to the discrepancies in the reported temperatures. Since this model predicts the number of ^{8}Li initially in the

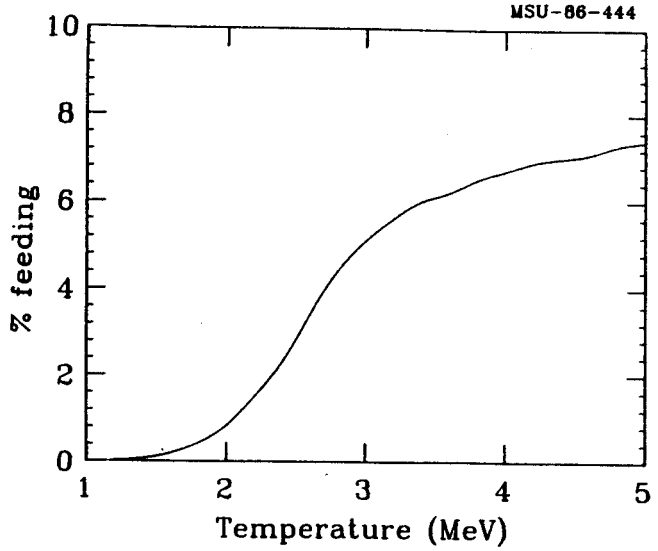

Fig. 2. Quantum-statistical model predictions for the feeding (in percent) of the ^{7}Li yield from the neutron decay of the 2.3 MeV state in ^{8}Li as a function of temperature (with parameters ρ/ρ_0=0.25 and Z/N=13/15).

For the temperature of 3 MeV (and the other model parameters unchanged) the model predicts that 33.5% of the observed ^{7}Li yield is from particle decay of other nuclei. The 0.478 MeV excited state to ground state population ratio, R, can be obtained from the observed excited state fraction, f, including feeding to the ground state, F_{gs}, from the relation:

$$R = \frac{f}{1 - f - F_{gs}} \qquad (3).$$

Then, the previously measured ^{7}Li bound excited state fraction[5] gives the ratio of the population of the first excited state to the ground state of ^{7}Li as 0.35±0.07 which (using Eq. (1)) corresponds to a temperature of $1.3^{+1.3}_{-0.5}$ MeV. This temperature is then consistent with that obtained by comparing the two excited state populations. Furthermore, the ratio of the population of the 7.456 MeV state to the ground state in ^{7}Li reported in Table I can be corrected for feeding in a similar manner. The values are shown in Table II. In each case, no attempt was made to include errors on the feeding of 33.5 percent. Considering the uncertainty in that value, it is reasonable to say that all three temperatures obtained from the populations of levels of ^{7}Li and the extent of the feeding to the ^{7}Li yield from the 2.255 MeV state in ^{8}Li are all consistent with a temperature of 2.5 to 3 MeV.

In conclusion, we have observed the 2.255 MeV state in ^{8}Li and the 7.456 MeV state in ^{7}Li from the reaction of ^{14}N+Ag at E/A=35 MeV via their neutron decay. The relative abundance of ^{7}Li in this excited state indicates a nuclear temperature of 3.0(4) MeV, significantly higher than observed in Refs. 4 and 5. The population of the 2.255 MeV state of ^{8}Li reflects a temperature of 1.6(3) MeV when the effect of sequential decay is ignored. Of all observed ^{7}Li, 6(2)% are from the neutron decay of the 2.255 MeV excited state in ^{8}Li, while 4(1)% of all ^{6}Li observed are from the neutron decay of the 7.456 MeV excited state in ^{7}Li.

In the case of ^{7}Li, measurements exist of the bound state populations, an unbound state population, and feeding from particle decay of another nucleus. All of these measurements are consistent with a single temperature of about 3 MeV when the effect of the total predicted feeding to the ground state from sequential decay is considered. This temperature is also consistent with charged-particle correlation measurements if one considers the 50° data with the E_1+E_2 range from 55 to 100 MeV of Ref. 3.

For the other isotopes for which bound state population measurements exist (^{6}Li, ^{8}Li, and ^{7}Be) such a complete picture does not exist. The only other measurement of feeding from sequential decay is from the 7.456 MeV state of ^{7}Li to the ground state of ^{6}Li. In light of the sucess in describing the ^{7}Li system, it is possible that the excited state populations of these other systems will also be understood in terms of temperature as more data becomes available.

TABLE II. Ratios, R, corrected for feeding via Eq. (3) and their corresponding temperatures, kT, according to Eq. (1).

States Compared	R (ratio)	kT (from R and Eq. (1))
^{7}Li(0.478)[a] to ^{7}Li(g.s.)	0.35(7)	$1.3^{+1.3}_{-0.5}$ MeV
^{7}Li(7.456) to ^{7}Li(g.s.)	0.11(3)	2.8(3) MeV

[a]Population of γ-emitting state from Ref. 5.

---

a. Present address, Lawrence Livermore National Laboratory, Livermore, CA, 94550.
b. Present address, Laboratoire GANIL, BP 5027, 14021 Caen Cedex, France.

References

1. D. J. Morrissey, W. Benenson, E. Kashy, B. Sherrill, A. D. Panagiotou, R. A. Blue, R. M. Ronningen, J. van der Plicht, and H. Utsunomiya, Phys. Lett. 148B,423(1984).
2. J. Pochodzalla, W.A. Friedman, C.K. Gelbke, W.G. Lynch, M. Maier, D. Ardouin, H. Delagrange, H. Doubre, C. Gregoire, A. Kyanowski, W. Mittig, A. Peghaire, J. Peter, F. Saint-Laurent, Y.P. Viyogi, B. Zwieglinski, G. Bizard, F. Lefebvres, B. Tamain, and J. Quebert, Phys. Rev. Lett. 55,177(1985); Phys. Lett. 161B,275(1985).
3. C.B. Chitwood, C.K. Gelbke, J. Pochodzalla, Z. Chen, D.J. Fields, W.G. Lynch, R. Morse, M.B. Tsang, D.H. Boal, and J.C. Shillcock, Phys. Lett. 172B,27(1986).
4. D.J. Morrissey, W. Benenson, E. Kashy, C. Bloch, M. Lowe, R. A. Blue, R. M. Ronningen, B. Sherrill, H. Utsunomiya, and I. Kelson, Phys. Rev. C 32,877(1985).
5. C. Bloch, W. Benenson, E. Kashy, D.J. Morrissey, R.A. Blue, R.M. Ronningen, and H. Utsunomiya, Phys. Rev. C 34,850(1986).
6. D. Hahn and H. Stöcker, LBL - preprint LBL-22378 (1986) and submitted to Nucl. Phys.
7. C. Bloch, Thesis, Michigan State University.
8. B.A. Remington, G. Caskey, A. Galonsky, C.K. Gelbke, L. Heilbronn, J. Heltsley, M.B. Tsang, F. Deak, A. Kiss, Z. Seres, J. Kasagi and J.J. Kolata, Phys. Rev. C 34,1685(1986).
9. R.J. Kurtz, University of California Radiation Lab Internal Report No. UCRL-11339,(1964).
10. A. Kiss, F. Deak, Z. Seres, G. Caskey, A. Galonsky, L. Heilbronn, B. Remington, and J. Kasagi, submitted to Phys. Lett.
11. B.V. Jacak, G.D. Westfall, C.K. Gelbke, L.H. Harwood, W.G. Lynch, D.K. Scott, H. Stöcker, M.B. Tsang, and T.J.M. Symons, Phys. Rev. Lett. 51,1846(1983).
12. F. Ajzenberg-Selove, Nucl. Phys. A413,1(1984).
13. H.M. Xu, D.J. Fields, W.G. Lynch, M.B. Tsang, C.K. Gelbke, M.R. Maier, D.J. Morrissey, J. Pochodzalla, D.G. Sarantites, L.G. Sobotka, M.L. Halbert, D.C. Hensley, D. Hahn, and H. Stocker, Phys. Lett. 182B,155(1986).
14. G. Fai and J. Randrup, Nucl. Phys. A404,551(1983) and L.P. Csernai, private communication.

SPALLATION AND FRAGMENTATION OF MEDIUM-A TARGETS BY HEAVY IONS

N.T. Porile[a], S.Y. Cho[a], Y.H. Chung[a] and D.J. Morrissey

We are investigating the interaction of 15-45 MeV/u C-12 ions with copper and silver by off-line gamma-ray measurements. During the past year, we performed experiments with 15 and 45 MeV/u C-12 ions. The data are presently being analyzed. Along with the results of earlier measurements with 25 and 35 MeV/u C-12 ions, the data will permit a determination of the evolution of the isobaric yield distribution, mass yield distribution, fragmentation yield, and momentum transfer with increasing bombarding energy.

---

a. Purdue University, W. Lafayette, IN

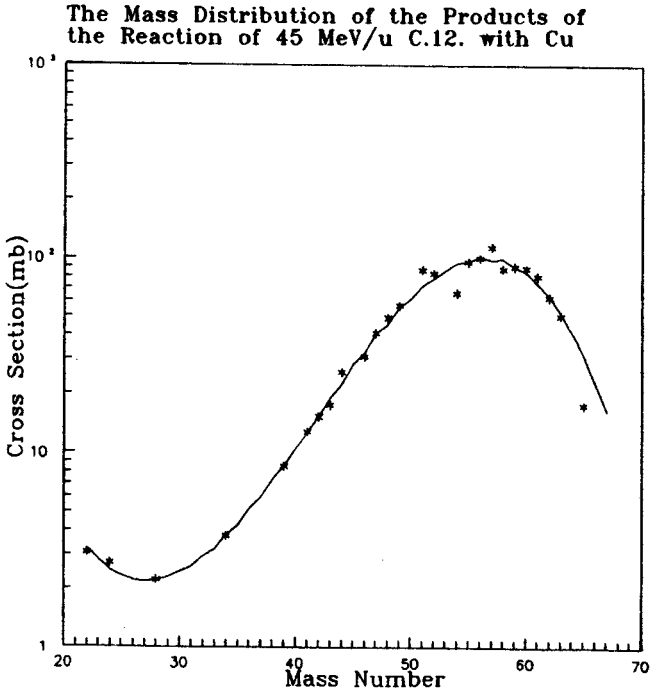

Fig. 1. The mass distribution of the products of the reaction of 45 MeV/u C.12. with Cu.

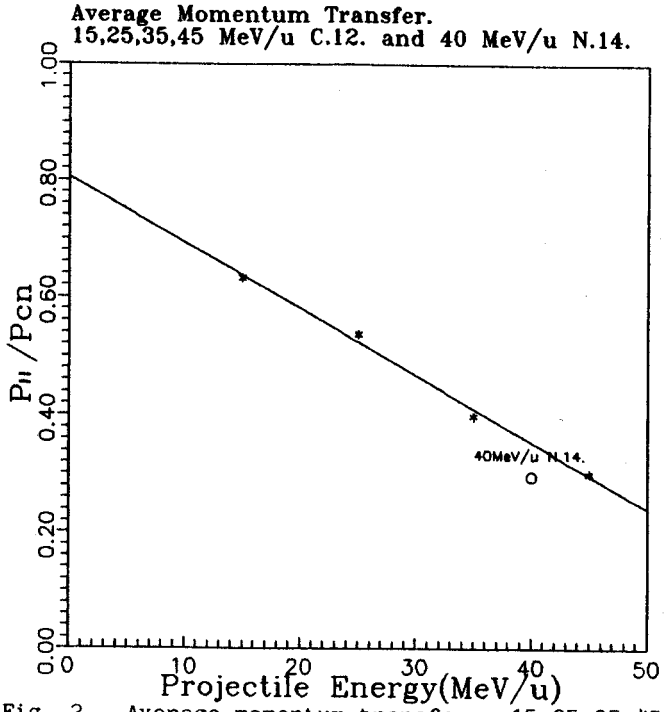

Fig. 2. Average momentum transfer. 15,25,35,45 MeV/u C.12. and 40 MeV/u N.14.

NUCLEAR FRAGMENTATION AND SEQUENTIAL DECAY

D.J. Fields, C.K. Gelbke, W.G. Lynch, and J. Pochodzalla[a]

Inclusive mass distributions from nuclear fragmentation reactions have catalyzed a number of theoretical speculations on the origin and significance of complex fragment emission from highly excited nuclear systems. Since many models of complex fragment emission neglect the populations of excited states and assume that fragmentation can be understood in terms of the ground state properties of emitted nuclei, we have investigated the modifications of primary particle distributions by the effects of sequential decays of particle unstable states. The population and subsequent decay of particle unstable states in complex nuclei can produce characteristic structures in the mass distributions similar to those observed [1] in high energy fragmentation reactions. Recent measurements of excited state populations [2-4] are consistent with statistical populations of nuclear states.

We assume that each available state, i, is initially populated with the weight, P_i, given by

$$P_i \propto P_0(A_i,Z_i)\ (2S_i+1)\ \exp(-E_i/T), \quad (1)$$

where $P_0(A_i,Z_i)$ denotes the population per spin degree of freedom of the ground state of a fragment of mass and charge numbers A_i and Z_i, respectively; S_i and E_i denote the spin and excitation energy of state i; T is the emission temperature which characterizes the statistical population of states of a given isotope. This temperature is, in general, different from the "kinetic" temperature which can be used to characterize energy spectra of the emitted fragments. In order to evaluate the effect of the decay of particle unstable states one has to specify the relative populations $P_0(A_i,Z_i)$. For simplicity, we use the parametrization:

$$P_0(A,Z) \propto \exp\{ -V_c/T + Q/T \} \quad (2)$$

where V_c is the Coulomb barrier for emission from a parent nucleus of mass and atomic numbers A_p and Z_p, and Q is the ground state Q-value:

$$V_c = Z_i(Z_p-Z_i)e^2/(r_o(A_i^{1/3}+ A_p^{1/3})) \quad (3)$$

and

$$Q = \{B(A_p-A_i,Z_p-Z_i) + B_i\} - B(A_p,Z_p) . \quad (4)$$

We used the radius parameter of r_o=1.2 fm. The binding energies, B(A,Z), of heavy nuclei are calculated from the Weizsäcker mass formula. For the emitted light fragments we use the measured binding energies, B_i, of the respective ground states. Alternative primary distributions could be explored; they will, however, not affect our qualitative conclusions.

We restrict our discussion to primary fragments of mass numbers $A_i \leq 20$. For these nuclei, all known [5] states with widths less than 3 MeV are included in the calculations. Particle unstable states are then allowed to decay statistically to available final states through the emission of light particles (n,p,d,t,^{3}He, and α particles).

Figure 1 shows the resulting primary mass distributions for emission from a moderately excited Xe nucleus (A_p=131, Z_p=54, and T=5 MeV). The histogram represents the total primary mass distribution including unbound states. The dark and light shaded regions represent the contribution from ground and excited particle stable states, respectively. Contributions from excited states dominate at this temperature.

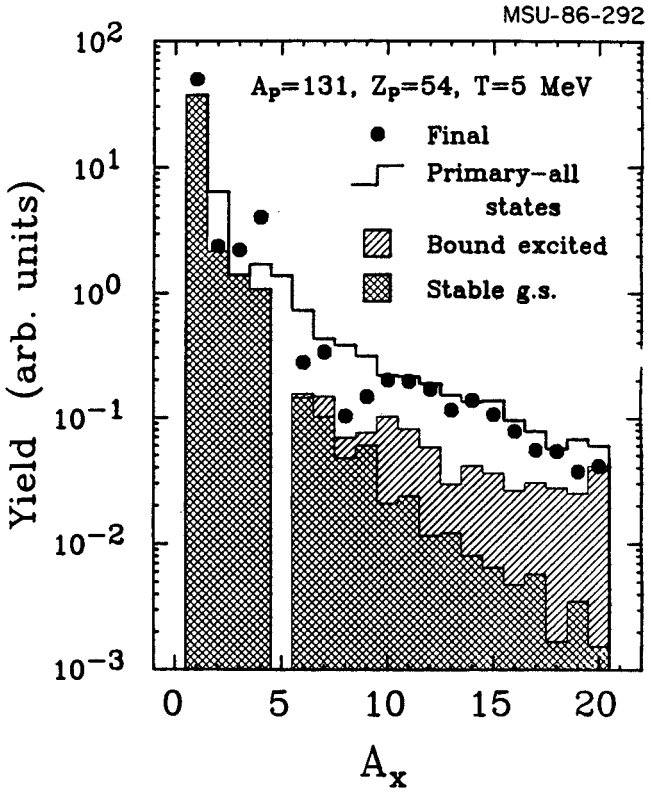

Fig. 1. Mass distributions calculated from Eqs. 1-4 for emission from a Xe nucleus at T=5 MeV. Histogram: primary distribution; open points: final distribution; dark and light shaded regions show contributions from bound ground and excited states, respectively.

The primary distributions are relatively smooth with little structure resulting from variations in level density and binding energies. The solid points in the figure show the final mass distribution after the decay of particle unstable states. These decays enhance the light particle yields; the yields of heavier fragments, A>4, are depleted by sequential decays. However, they remain significantly larger than the primary yields of bound nuclei. Approximately half of the fragment yield is attributable to secondary decays.

Figure 2 compares the calculated final mass distribution (histogram) with the distribution measured [1] for proton-induced reactions on Xe at E_p=80-350 GeV (solid points). (The calculated mass distribution includes only nuclei for which cross sections were published in ref. 4, and differs from the final distribution in Figure 1 principally by the exclusion of ^{6}He.) The calculation at this temperature, T=5 MeV, reproduces the average slope of the mass distribution. In addition, the calculation reproduces the characteristic structures in the experimental mass distribution for nuclei 6≤A≤14.

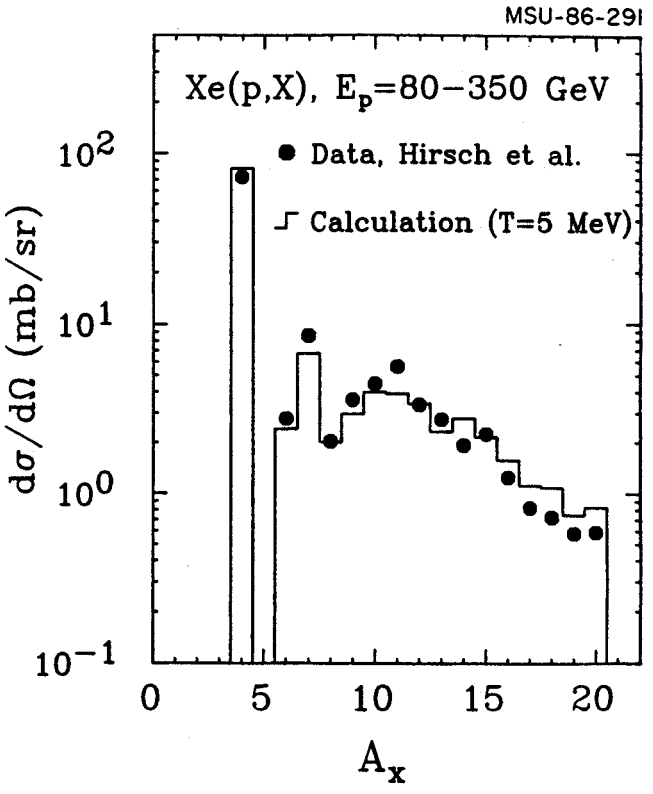

Fig. 2. Mass distribution [1] from proton induced reactions on Xe (solid points) and final distribution predicted from Eqs. 1-4 (histogram).

Direct measurements of the relative populations of nuclear states in intermediate energy nucleus-nucleus collisions have provided puzzling results. In thermal models, the ratio of the primary populations of two narrow states, i and j, in a given nucleus is given by

$$R_p = \frac{P_i}{P_j} = R_\infty \exp(-\Delta E_{ij}/T)$$

$$= \frac{(2s_i+1)}{(2s_j+1)} \exp(-\Delta E_{ij}/T) \quad , \quad (5)$$

where ΔE_{ij} is the difference in the level energies and R_∞ is the high temperature limit.

This expression was used to extract the effective emission temperatures from the measured relative populations of excited states [2-4,6-8]. The populations of low lying particle stable levels relative to the respective ground states were interpreted [6,7] in terms of unexpectedly low emission temperatures, T<1 MeV. Measurements of populations of particle unstable levels [2-4,8] indicated higher average emission temperatures of about 5 MeV. It has been suggested [2,4,8,9] that sequential decay is responsible for discrepancies between these measurements.

We have calculated the primary and final population ratios, R_p, for several previously analyzed [2-4,8] particle unbound levels in ^{4}He, ^{5}Li, ^{6}Li, and ^{8}Be nuclei. The dotted curves in Fig. 3 show the temperature dependences of the primary population ratios given by Eq. 5. The solid curves indicate the final population ratios when one includes the sequential decays of excited primary fragments populated according to Eqs. 1-4. At low emission temperatures, T≤1 MeV, few unbound states are populated; the primary and final population ratios are equivalent, and Eq. 5 can be used to determine emission temperatures. At higher temperatures, however, the final populations do not follow the thermal relation of Eq. 5. Instead, they reflect the feeding from higher lying levels. All population ratios are predicted to reach saturation values less than expected from the simple relation of Eq. 5. The calculations corroborate the qualitative arguments given in ref. 2 that Eq. 5 can only be used to determine emission temperatures when ΔE/T<<1. However, even in such cases problems can arise; see, for example, the predicted strong perturbation of the ratio of the 3.04 and 17.6 MeV levels in ^{8}Be. Of the six examples shown in Figure 3, the ^{5}Li population ratio is the only case which is predicted to be relatively unperturbed by secondary decays for temperatures up to T≤10 MeV.

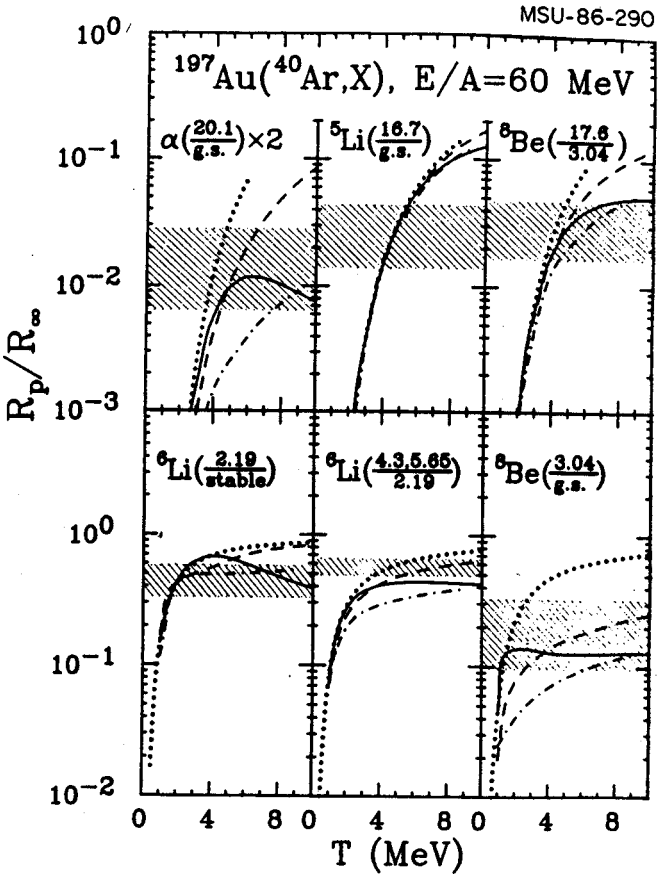

Fig. 3. Temperature dependence of population ratios, R_p/R_∞, for specific states in ^{4}He, ^{5}Li, ^{6}Li, ^{8}Be nuclei. Ratios measured for the ^{40}Ar+^{197}Au reaction at E/A=60 MeV are shown by hatched regions [2-4]. Dotted curves: temperature dependence of primary population ratios; solid curves: final ratios predicted from Eqs. 1-4; dashed and dashed-dotted curves: final ratios predicted by quantum statistical calculations [10] for densities of ρ/ρ_0= 0.05 and 0.9, respectively.

The effects of sequential decay are influenced by two factors: the relative populations of excited states and the distribution $P_0(A_i,Z_i)$. For steeply falling primary mass distributions, the population ratios will be less modified by sequential decay processes than for flat primary mass distributions. Mass distributions calculated from Eqs. 2-4 become flatter at higher temperatures. This increases the modifications of the population ratios. In order assess the differences which exist for different

distributions of primary fragments we also show the results of quantum statistical calculations [10]. Penetration through the Coulomb barrier is neglected in this model. The mass distributions become steeper with increasing temperature and with decreasing breakup density, ρ. The dashed and dashed-dotted curves in Fig. 3 show final population ratios predicted for breakup densities of $\rho/\rho_0 = 0.05$ and 0.9, respectively, where ρ_0 is the ground state nuclear density.

The shaded areas in Fig. 3 give the relative populations of states measured [2-4] for ^{40}Ar induced reactions on ^{197}Au at E/A=60 MeV. Within the present theoretical uncertainties concerning the primary fragment distribution and the branching ratios for the decays of many of the high lying states, the experimental population ratios are consistent with an equilibrium primary population of excited states at a temperature of T≈4-5 MeV. Further specification of the primary distribution will only be possible with additional constraints provided by elemental and isotopic distributions.

---

a. Present address: Institut für Kernphysik, J.W. Goethe Universität, 6000 Frankfurt 90 (W.Germany).

References

1. A.S. Hirsch et al., Phys. Rev. C29 (1984) 508.
2. J. Pochodzalla et al., Phys. Rev. Lett. 55 (1985) 177.
3. J. Pochodzalla et al., Phys. Lett. 161B (1985) 275.
4. J. Pochodzalla, et al., Phys. Rev C (in press).
5. Ajzenberg-Selove, Nucl. Phys. A449 (1986) 1, and references therein.
6. D.J. Morrissey et al., Phys. Lett. 148B (1984) 423.
7. D.J. Morrissey et al., Phys. Rev. C32 (1985) 877.
8. C.B. Chitwood et al., Phys. Lett. 172B (1986) 27.
9. H. Xu et al., Phys. Lett. 182B (1986) 155.
10. D. Hahn and H. Stöcker, LBL preprint LBL-22378.

FRAGMENTATION STUDIES OF ^{18}O ON ^{58}Ni AT FORWARD ANGLES

M.M. Torres, S.P. Angius, D. Cebra, G.M. Crawley, D. Fox, A. Machiavelli[a], Menchaca-Rocha[b], A. Pradham, A. Toledo[c], G.D. Westfall and K. Wilson

Much of the recent work done on heavy-ions reactions at energies above 20 Mev/nucleon has focussed on the emission of light particles or has selected high multiplicity events which are thought to arise from central collisions. For more peripheral collisions, on the other hand, the transfer of one or more nucleons from the projectile to the target, and projectile fragmentation have been suggested as possible reaction mechanisms. These processes can in principle be distinguished by their different angular distributions. It is therefore important to be able to measure angular distributions for different fragments down to very forward angles, and to make an accurate identification (Z and M) of the particles observed.

This motivated us to perform a series of measurements with the S320 spectrograph, using both ^{16}O and ^{18}O beams of 35 Mev/nucleon on a ^{58}Ni target. Projectile like fragments were measured between laboratory angles of 2 and 10 degrees in 1 degree steps. Since the energy range which had to be covered was very large, it was necessary to take a large number of momentum "bites", in some cases 6-8, to obtain a fairly complete spectrum. Using the energy loss in the gas ionization chamber in the S320 focal plane, the light from the scintillator behind the ionization chamber and the time of flight of emitted particles through the spectrograph, it was possible to cleanly separate isotopic masses up to 18.

A number of complete momemtum spectra have been obtained. Two examples of such spectra for ^{14}C and ^{15}N measured at 6 degrees are shown in Figures 1a and ab. Both of these spectra show broad peaks centered just below the beam energy. The data from this experiment are being analyzed at the Tandar Lab, Buenos Aires and at the Instituto de Fisica, Sao Paulo.

---

a. Instituto de Fisica, Buenos Aires.
b. Instituto de Fisica, U.N.A.M
c. Instituto de Fisica, Sao Paulo

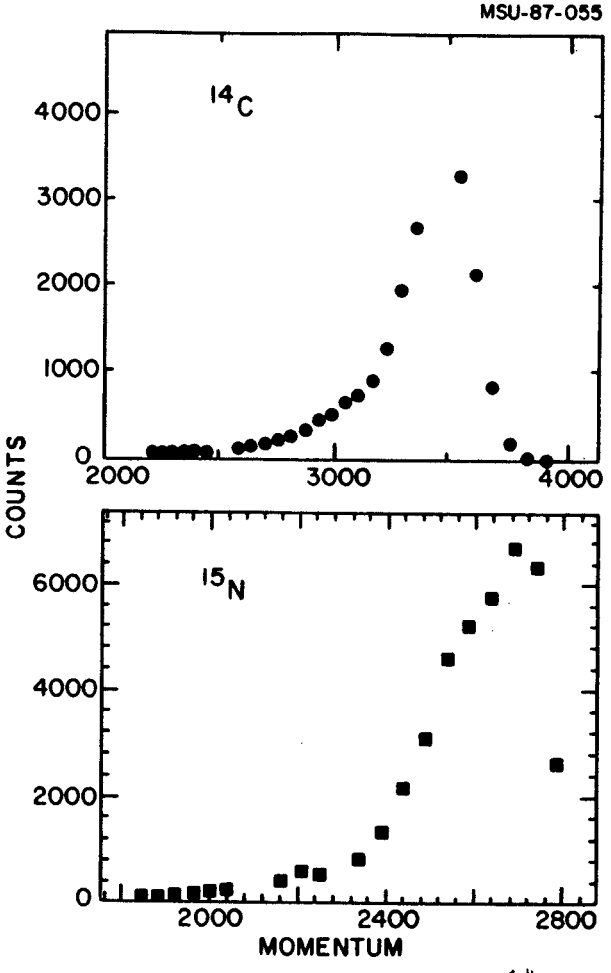

Fig. 1a Momentum spectrum for ^{14}C at 6 degrees.

Fig. 1b Momentum spectrum for ^{15}N at 6 degrees.

DEPENDENCE OF TWO-PARTICLE CORRELATION FUNCTIONS ON LINEAR MOMENTUM TRANSFER TO COMPOSITE SYSTEM

Z. Chen, C.K. Gelbke, J. Pochodzalla[a], C.B. Chitwood, D.J. Fields, W.G. Lynch, and M.B. Tsang

Because of their sensitivity to final state interactions and quantum statistics, light particle correlations at small relative momenta contain information about the space-time characteristics of the emitting system [1-3]. While two-particle inclusive measurements can provide insights about the average properties of the emitting system, more detailed information must be obtained from more exclusive measurements in which specific classes of reactions can be suppressed or enhanced. We used the linear momentum transferred to the heavy reaction residue as a filter to discriminate between quasi-elastic and more violent, fusion-like projectile-target interactions and investigated two-particle correlation functions at small relative momenta for these two types of reactions. The maxima of the p-p and α-d correlation functions are larger for fusion-like reactions than for quasi-elastic collisions.

A 1.1 mg/cm^2 thick gold target was irradiated by ^{14}N ions with E/A=35 MeV incident energy. Light particles (Z≤2) were detected by a close-packed hexagonal array of 13 ΔE-E telescopes, each consisting of a 400 μm thick Si detector and a 10 cm thick NaI detector. Coincident fission fragments were detected with two X-Y-position sensitive parallel plate detectors.

The left hand part of Fig. 1 shows folding angle distributions, $\Theta_{ff}=\Theta_A+\Theta_B$, where Θ_A and Θ_B denote the polar angles of the two coincident fission fragments. The upper scale indicates the average linear momentum, Δp/p, transferred to the heavy reaction residue (measured in units of the projectile momentum, p). Open points correspond to the inclusive folding angle distribution; full points represent the

MSU-86-203

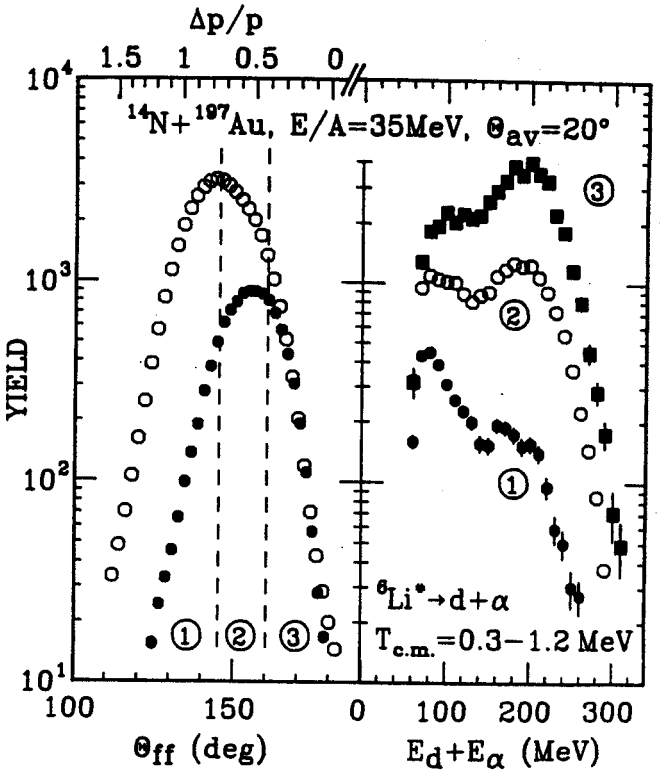

Fig. 1. Left hand part: Folding angle distributions measured inclusively (open points) and in coincidence with α-d pairs (full points). The dashed lines indicate the boundaries for gates (1), (2) and (3). Right hand part: Dependence of the α-d coincidence yield on the total kinetic energy, E_d+E_α, for α-d pairs which can be attributed to the 2.186 MeV state in ^{6}Li. The spectra are gated as indicated. The vertical scale is in arbitrary units.

distribution measured in coincidence with α-d pairs. The inclusive distribution exhibits a maximum at Δp/p≈0.8, indicating dominant contributions from incomplete fusion reactions. Small folding angles are suppressed when coincident α-d pairs are detected in the light-particle hodoscope. To a large extent, this suppression is due to momentum conservation: the coincident α-d pairs carry away an average linear momentum of 0.35p.

In order to explore the dependence of light particle energy spectra and correlation functions on the linear momentum transferred to the heavy target residue, we have used three gates on folding angle. (Gate (1): θ_{ff}<145°; gate (2): θ_{ff}=145°-160°; gate (3): θ_{ff}>160°.) The right hand side of Fig. 1 shows the dependence of the α-d coincidence yield on the total kinetic energy, E_d+E_α, for α-d pairs which can be attributed to the 2.186 MeV state of ^{6}Li ($E_{rel}=q^2/2\mu$=0.3-1.2 MeV). For small linear momentum transfers (gate (3): θ_{ff}>160°), the α-d coincidence yield is dominated by a strong quasi-elastic component centered close to the projectile velocity. This component is strongly suppressed by gating on large linear momentum transfers (gate (1): θ_{ff}<145°). In general, large linear momentum transfers to the heavy reaction residue can serve as an effective filter condition to suppress quasi-elastic components in the energy spectra.

The two-particle correlation function, R(q), is defined in terms of the singles yields, $Y_1(\vec{p}_1)$ and $Y_2(\vec{p}_2)$, and the coincidence yield, $Y_{12}(\vec{p}_1,\vec{p}_2)$, of particles 1 and 2:

$$\sum Y_{12}(\vec{p}_1,\vec{p}_2) = C_{12}\cdot[1+R(q)]\cdot\sum Y_1(\vec{p}_1)Y_2(\vec{p}_2) \ .$$

Here, $\vec{p}_1$ and $\vec{p}_2$ are the momenta of the two detected particles, q is the momentum of relative motion, and C_{12} is a normalization constant which is chosen such that the average correlation function, <R(q)>, vanishes for sufficiently large q, where correlations due to final state interactions become negligible. For each gate on θ_{ff} and E_1+E_2, the sum was extended over all energy and detector combinations corresponding to the given relative momentum, q.

Figures 2 and 3 show the α-d and p-p correlation functions measured for large (gate (1), open points) and small (gate (3), solid points) linear momentum transfers to the heavy reaction residue. In order to reduce contributions from later stages of the reaction

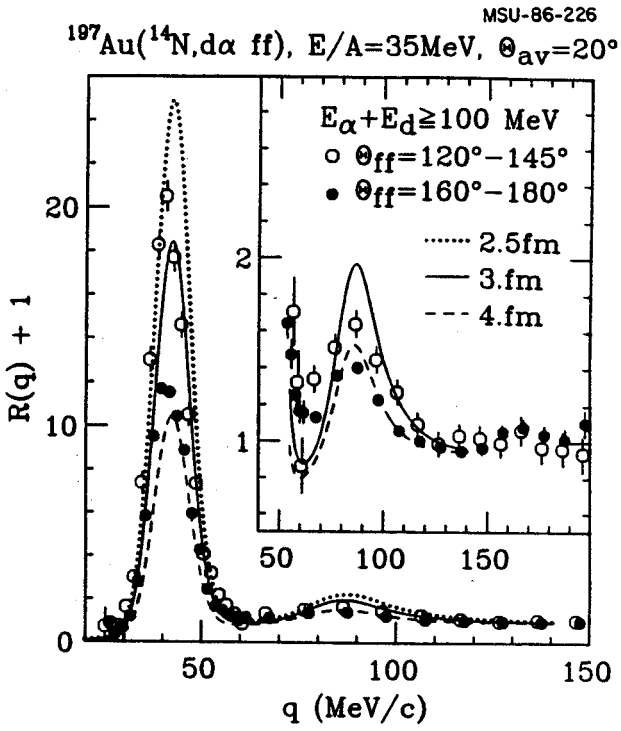

Fig. 2. α-d correlation functions gated on large (gate (1): open points) and small (gate (3): solid points) linear momentum transfers to the heavy reaction residue. The gate on the total kinetic energy is indicated in the figure; the curves are explained in the text.

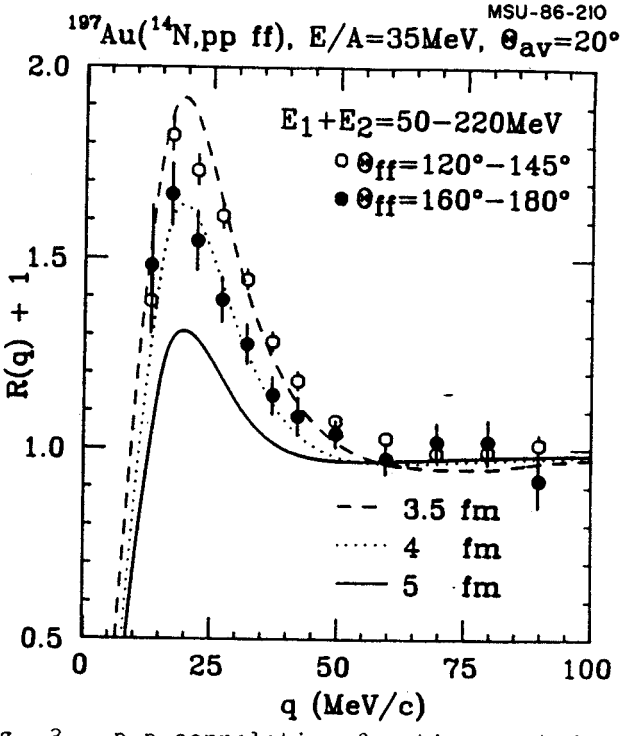

Fig. 3. p-p correlation functions gated on large (gate (1): open points) and small (gate (3): solid points) linear momentum transfers to the heavy reaction residue. The gate on the total kinetic energy is indicated in the figure; the curves are explained in the text.

for which sequential emission of low energy particles from the fully equilibrated composite system may be important, these correlations were gated on total energies well above the compound nucleus Coulomb barrier: $E_\alpha+E_d \geq 100$ MeV and $E_{p1}+E_{p2} \geq 50$ MeV. (The dependence of the α-d correlation function on the total energy, $E_\alpha+E_d$, is shown in Fig. 4.) The selection of events with large linear momentum transfer produces enhanced maxima in both correlation functions as compared to those with low momentum transfer.

MSU-86-204

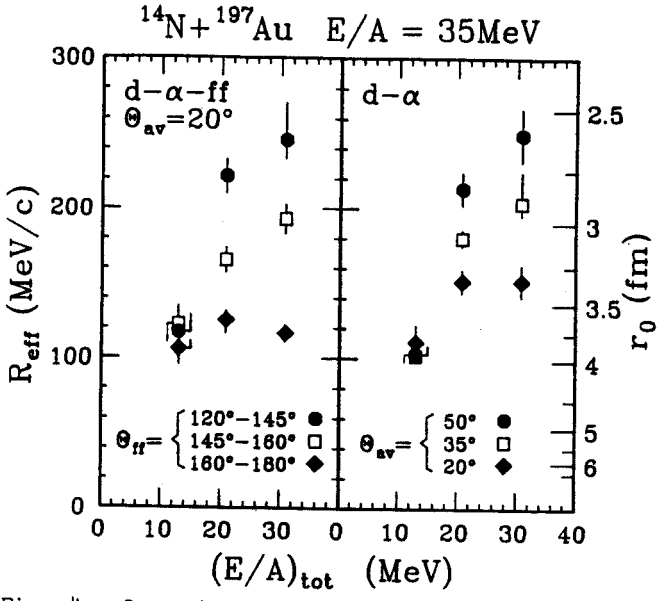

Fig. 4. Dependence of α-d correlations on the total energy per nucleon, $(E/A)_{tot}=(E_\alpha+E_d)/6$, of the two coincident particles. Correlations measured inclusively and in coincidence with fission fragments are shown in the right and left hand parts, respectively. The left hand scale corresponds to $R_{eff}=\int dq \cdot R(q)$, with the integration performed over the range of q=30-60 MeV. The right hand scale gives source radii extracted with the model of ref. 2.

For the α-d correlation function, the sharp peak at q≈42 MeV/c is enhanced by about a factor of two. For the p-p correlation function, the enhancement is less dramatic but still appreciable.

The curves shown in Figs. 2 and 3 represent theoretical correlation functions predicted by the final-state interaction model of ref. 1 and its extension [2] to particles heavier than protons. The emitting system was assumed to have a Gaussian density distribution, $\rho(r) \propto \exp(-r^2/r_0^2)$, and negligible life-time. In this approximation, the model becomes equivalent with the thermal model [3]. Source radii extracted under this assumption of instantaneous emission represent upper limits for the spatial extent of the emitting system [1,2].

For the case of p-p correlations, source radii of $r_0 \approx 3.7$ and 4.0 fm are extracted for gates (1) and (3), respectively. Source radii extracted from the sharp peak of the α-d correlation function at q≈42 MeV/c are $r_0 \approx 2.8$ and 3.6 fm, respectively, for gates (1) and (3). (Source radii extracted from the broad peak of the α-d correlation function at q ≈ 85 MeV/c are larger by about 0.8 fm.) The extracted source sizes are generally smaller than the size of the target nucleus ($r_0(Au) = \sqrt{2/3} \cdot r_{rms}(Au) \approx 4.4$ fm).

A strictly geometric interpretation of our results would imply that quasi-elastic collisions are characterised by sources significantly larger than the size of the projectile nucleus ($r_0(N) \approx 2.1$ fm). It is, however, likely that temporal effects cannot be neglected when interpreting these results. The time scales characteristic of preequilibrium particle emission in violent fusion-like collisions may be shorter than those which characterize particle emission in quasi-elastic reactions thus producing stronger correlations and smaller apparent source radii. Our observation of reduced correlations for peripheral processes may, therefore, reflect longer emission time scales rather than larger source dimensions. The sequential decay of excited projectile residues is an example for reactions which proceed via longer emission time scales. For such processes, Koonin's formulation may be less useful for the calculation of two-particle correlation

functions and alternative statistical formulations, such as appropriate generalisations of the Hauser Feshbach theory, could be explored. For the case of equilibrium decay of light compound nuclei, Hauser Feshbach calculations [4] have predicted smaller two-proton correlations than expected from the zero-lifetime limit of Koonin's model. Within Koonin's model, reduced correlations are expected due to the long lifetime of the compound nucleus. From these arguments, one expects reduced correlations for peripheral collisions for which contributions from the decay of equilibrated projectile residues may be important. For the emission of energetic particles in fusion-like collisions such processes are suppressed. It is significant that these collisions exhibit larger correlations. They should reflect, more clearly, the space-time localisation of the reaction.

Figure 4 shows the dependence of α-d correlations on the total energy per nucleon, $(E/A)_{tot}=(E_\alpha+E_d)/6$, of the two coincident particles. Inclusive correlations and correlations measured in coincidence with fission fragments are shown in the right and left hand parts of the figure, respectively. The left hand scale of the figure gives the integral correlation, $R_{eff}=\int dq \cdot R(q)$. The right hand scale of the figure gives source radii extracted with the model of ref. 2. At low energies, the α-d correlations are of comparable magnitude. For small linear momentum transfers (gate 3), they are nearly independent of energy. On the other hand, the α-d correlations for larger linear momentum transfers vary strongly with energy. For inclusive correlations, right hand part of Figure 4, a similar energy dependence exists and becomes more pronounced at larger angles, Θ_{av}, where contributions from quasi-elastic processes become less important.

---

a. Present address: Institut für Kernphysik, J.W. Goethe Universität, August-Euler-Straße 6, 6000 Frankfurt, W-Germany

References

1. S.E. Koonin, Phys. Lett. 70B (1976) 43.
2. D.H. Boal and J.C. Shillcock, Phys. Rev. C33 (1986) 549.
3. B.K. Jennings, D.H. Boal, and J.C. Shillcock, Phys. Rev. C33 (1986) 1303.
4. M.A. Bernstein, W.A. Friedman, W.G. Lynch, C.B. Chitwood, D.J. Fields, C.K. Gelbke, M.B. Tsang, T.C. Awes, R.L. Ferguson, F.E. Obenshain, F. Plasil, R.L. Robinson, and G.R. Young, Phys. Rev. Lett. 54 (1985) 402.

EXTERNAL COULOMB DISTORTION OF PROTON-DEUTERON FINAL-STATE INTERACTIONS FOR ^{14}N INDUCED REACTIONS ON ^{197}Au AT E/A=35 MeV

J. Pochodzalla, C.K. Gelbke, C.B. Chitwood, D.J. Fields, W.G. Lynch, M.B. Tsang, and W.A. Friedman[a]

Correlations between two particles which experience non-resonant final-state interactions and which have different mass-to-charge ratios are sensitive to the Coulomb field of the residual nuclear system at the point of emission. This sensitivity is derived from the absence of long-lived final states and the different accelerations of the particles in the Coulomb field. We have investigated the distortion of proton-deuteron correlations resulting from the close proximity of the target-like residue at the point of emission for ^{14}N induced reactions on ^{197}Au at E/A = 35 MeV.

A gold target of 19 mg/cm^2 areal density was irradiated with ^{14}N ions of E/A = 35 MeV. Light particles ($Z \leq 2$) were detected by a closed-packed hexagonal array of 13 ΔE-E telescopes, each consisting of a 400 μm thick Si-detector and a 10 cm long NaI-detector. Each telescope subtended a solid angle of 0.94 msr; the angular separation between adjacent telescopes was 6.1°. The overall energy calibration for hydrogen isotopes is accurate to within 3% for E/A ≤ 25 MeV and within 2% for E/A ≈ 25-50 MeV.

We define the two-particle correlation function, $R(E_p, E_d, \Delta\theta)$, in terms of the coincidence and singles yields:

$$\sum Y_{pd}(E_p, \vec{n}_p, E_d, \vec{n}_d) = C\cdot\{1+R(E_p,E_d,\Delta\theta)\}\cdot\sum Y_p(E_p,\vec{n}_p)\cdot Y_d(E_d,\vec{n}_d) \quad (1)$$

The indices p and d denote protons and deuterons, respectively; E is the energy and $\vec{n}$ is a unit vector parallel to the velocity of the detected particle; C is a normalization constant and $\cos(\Delta\theta)=\vec{n}_p\cdot\vec{n}_d$. The summation in eq. (1) is performed over all energies and angles corresponding to the given bins of E_p, E_d, and Δθ.

A two-dimensional plot of the p-d correlation function for fixed relative angles of Δθ = 6.1° reveals a clear minimum for small relative velocities, $\vec{v}_p \approx \vec{v}_d$, which is caused by the repulsive proton - deuteron Coulomb interaction. The exact location of the minimum is, however, displaced from the line $v_p = v_d$. For a more quantitative analysis, we introduce new coordinates T and S measured along axes parallel and perpendicular to the line $v_p = v_d$ (i.e. $E_d=\alpha\cdot E_p$):

$$S = (\alpha\cdot E_p - E_d)/\sqrt{1+\alpha^2} \quad ,$$
$$T = (E_p + \alpha\cdot E_d)/\sqrt{1+\alpha^2} \quad . \quad (2)$$

In terms of these coordinates, the line $E_d=\alpha\cdot E_p$ corresponds to S=0.

By analogy with eq. (1), we now define the correlation function R(S):

$$\sum \int_{T_1}^{T_2} dT\cdot Y_{pd}(S,T) = C\cdot\{1+R(S)\}\cdot\sum \int_{T_1}^{T_2} dT\cdot Y_p[E_p(S,T)]\cdot Y_d[E_d(S,T)]. \quad (3)$$

Figure 1 shows R(S) measured for θ_{av}=35° and 50°. Energy thresholds $E_p \geq 12$ MeV and $E_d \geq 15$ MeV were applied to the summation in addition to the constraints on T. The values, S_0, corresponding to minimum relative velocity are marked by the dotted lines. The locations, S_c, of the minima of the correlations functions, R(S), are shown in Fig. 2a. No significant energy or angle dependence is observed; the average value is $\bar{S}_c = 2.6\pm0.8$ MeV.

We have performed three-body Coulomb trajectory calculations. Correlation functions

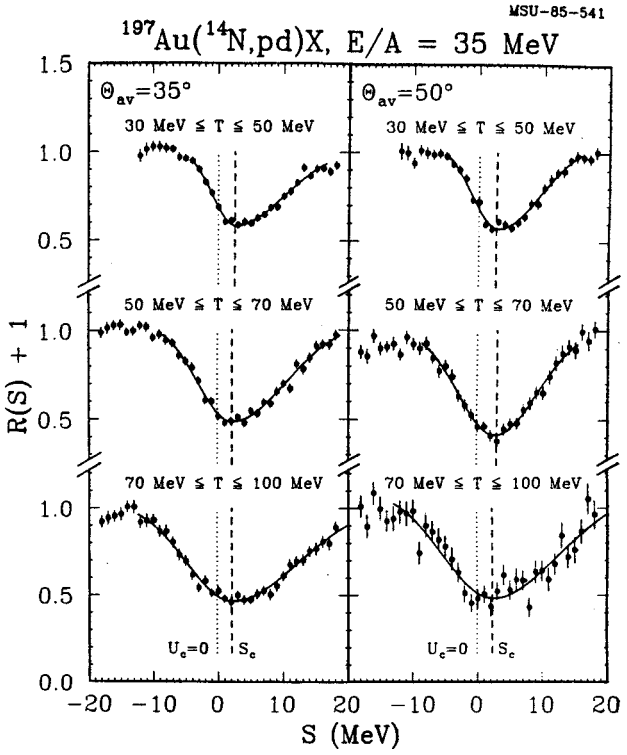

Fig. 1. Correlation function for coincident protons and deuterons as a function of the coordinate S (eq. 2). The lines are explained in the text.

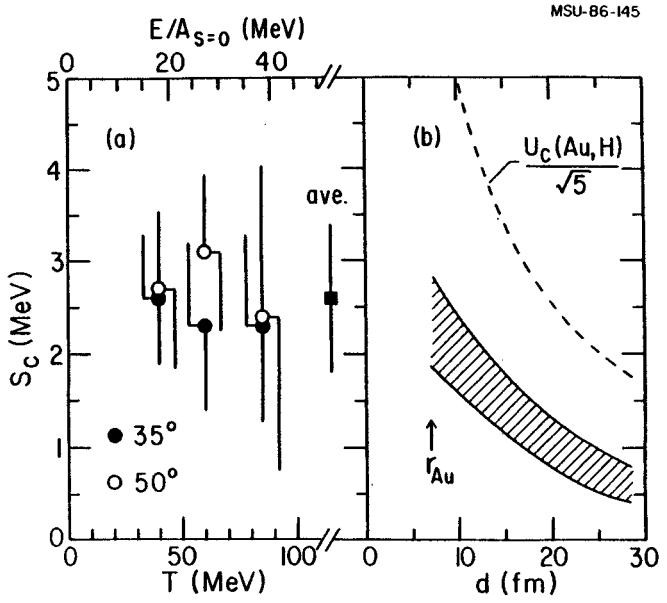

Fig. 2. Part a: Extracted shifts S_c for different values of the coordinate T (eq. 2). The upper scale gives energies per nucleon at S=0. Part b: Displacement S_c calculated as a function of the distance of emission, d, with respect to a Au nucleus.

were generated by means of a Monte Carlo sampling of the initial conditions. Protons and deuterons were assumed to be emitted simultaneously from a dilute source of Gaussian spatial probability distribution, $N(\vec{r}) \sim e^{-(\vec{r}-\vec{d})^2/r_0^2} \cdot d^3r$; a source size of r_0 = 5 fm was used. The source was located at a distance d from the center of the target nucleus.. The initial velocities of the emitted particles were assumed to be distributed as $N(\vec{v}) \sim e^{-m(\vec{v}-\vec{v}_0)^2/2T_0} \cdot d^3v$; the parameters $\vec{v}_0 = \frac{1}{2} \cdot \vec{v}_{beam}$ and T_0 = 10 MeV were used (see ref. 1 for details). The Coulomb interaction with the dilute source was neglected: only the Coulomb forces between the proton, deuteron and the target nucleus were taken into account.

In agreement with the experimental observation, the calculated location of the minimum of R(S) was found to be rather insensitive to the laboratory angle, Θ_{av}, or to the total kinetic energy of the emitted particles. The hatched region in fig. 2b shows, therefore, only the energy and angle integrated shifts, S_c, as a function of the distance d. The width of this band represents variations of S_c resulting from conceivable changes of the source parameters. The experimental shift, $\bar{S}_c$, indicates a distance of emission d < 15 fm. This is consistent with emission from a point close to the surface of the composite system and excludes significant contributions to the yield of coincident protons and deuterons from the sequential decay of long-lived projectile fragments.

---

a. Department of Physics, University of Wisconsin, Madison, WI.

References

1. J. Pochodzalla et al., Phys. Lett. 175B (1986) 275.

MULTIPLICITY DEPENDENT LIGHT PARTICLE CORRELATIONS

J. Pochodzalla, C.K. Gelbke, W.Lynch, M. Maier, A. Kyanowski[a], F. Saint-Laurent[a], D. Ardouin[a], H. Delagrange[a], H. Doubre[a], C. Gregoire[a], W. Mittig[a], A. Peghaire[a], J. Peter[a], Y.P. Viyogi[a], B. Zwieglinski[a], J. Quebert[b], G. Bizard[c], F. Lefebvres[c] and B. Tamain[c]

Information about the size of an emitting source can be obtained from light particle intensity interferometry[1]. We have measured correlations between deuterons and alpha particles in coincidence with light particles detected at forward angles in a large multidetector system.

The experiment was performed at the Laboratoire National GANIL in Caen (France). A gold target of 10 mg/cm^2 areal density was irradiated by an ^{40}Ar beam at an incident energy of E/A = 60 MeV. Light particles (Z < 3) were detected by a closely packed hexagonal hodoscope[2] of 13 Si-NaI (400 μm and 10 cm thick) telescopes. The angular separation between adjacent elements was 4.2°, each telescope subtending a solid angle of 0.46 msr. This hodoscope was centered at a laboratory angle of 30°. In order to select an event type, coincident light particles were detected in a multidetector array consisting of 96 2mm-thick plastic scintillators (plastic wall) arranged in a circular array of seven rings around the beam axis. The charge and the velocity of each light particle were determined by a ΔE-time-of-flight measurement. For the present experiment, the plastic wall covered an angular range of 5° < θ < 30° in the laboratory frame; its detection threshold was about 4 MeV/nucleon for protons and alpha particles, significantly below the corresponding average kinetic energies observed in this experiment.

The data taken with the hodoscope are presented in terms of the correlation function R(q), defined for a particle pair (1,2) by

$$Y_{1,2}(p_1,p_2)=CY_1(p_1)Y_2(p_2)[1+R(q)], \qquad (1)$$

where $Y_{1,2}$ denotes the coincidence yield, Y_1 and Y_2 the singles yields. The laboratory momenta of particles 1 and 2 are p_1 and p_2 respectively, and q is the momentum of relative motion. The normalization constant C is determined by the requirement that R(q) = 0 at large relative momenta (150 < q < 200 MeV/c). For event-selection using the plastic wall, the same constraint is applied to the coincidence and the single yields.

Coincident data with the plastic wall provide information on the degree of violence of the reaction. We have explored the effects of the observed charged particle multiplicity on the light particle correlations. The dependence of the α-d correlation function on the number, of coincident charged particles detected in the plastic wall is shown in Fig. 1.

For ν=0, the magnitude of the sharp peak of the α-d correlation function is larger than about a factor of 3-4 as compared to the magnitude for ν=10. Between these two extremes, the maximum of the correlation function decreases smoothly with increasing multiplicity as shown in Fig. 2. The right hand side of the figure shows some dimensions extracted from the final-state interaction model[1,2] assuming a source of Gausian density distribution and negligible lifetime. The largest value of r_0 = 8 fm means that the decay of the system occurs either at low density (~0.5 ρ_0 if all incoming nucleons contribute) or over a non-negligible time interval.

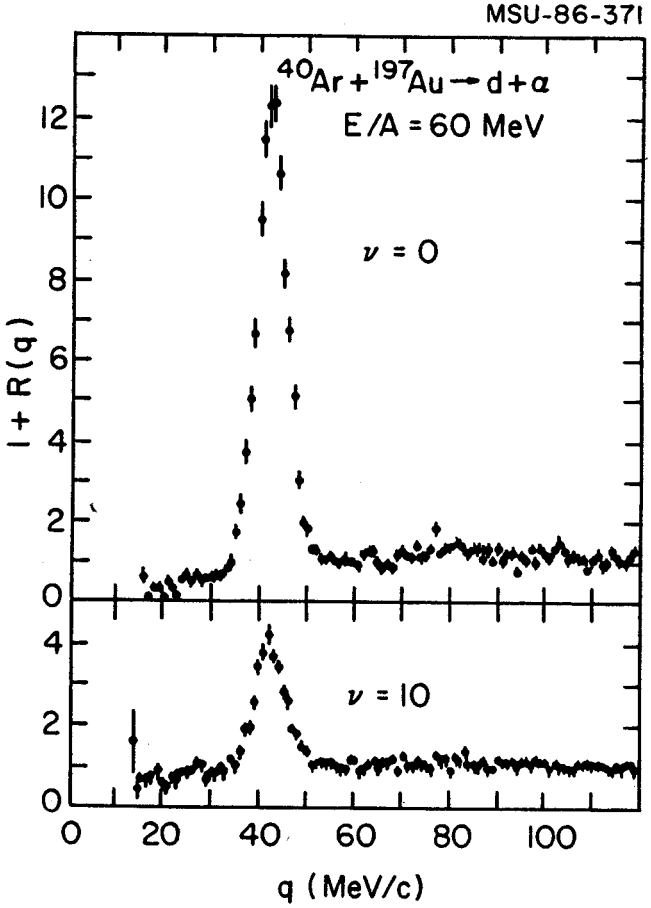

Fig. 1. d-α correlation function versus relative momentum q: (a) without any selection in the plastic wall, (b) for zero multiplicity (M = 0), (c) for M = 10. Equally shown are theoretical calculations (12) for r_o = 4, 5 and 8 fm.

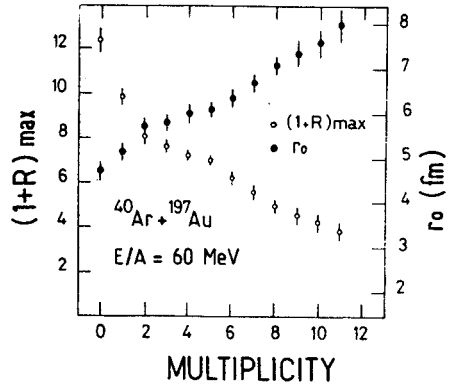

Fig. 2. Evolution of the maximum of the d-α correlation function (open circles) and the derived spactime parameter r_o (full circles) as a function of the detected multiplicity.

a. Laboratoire National GANIL, Caen Cedex, France
b. Centre d'Estudes Nucleaires de Bordeaux, Gradignan, France
c. Laboratoire de Physique Corpusculaire Caen Cedex, France

References

1. S.E. Koonin, Phys. Lett. 70B(1977)43.
2. D.H. Boal and J.C. Shillcock, Phys. Rev. C33(1986)549.

SOURCE PROPERTIES OF INTERMEDIATE MASS FRAGMENTS EMITTED IN THE E/A = 35 MeV ^{14}N + ^{232}Th REACTION

M. Fatyga,[a] K. Kwiatkowski,[a] V.E. Viola,[a] W.G. Wilson,[a] M.B. Tsang, J. Pochodzalla, W.G. Lynch, C.K. Gelbke, D.J. Fields and C.B. Chitwood

We have investigated the emission of intermediate mass fragments (IMFs) in the ^{14}N-induced reaction on ^{232}Th in order to characterize the sources from which these fragments are emitted and to investigate whether equilibrium and non-equilibrium components could be associated with different classes of collisions. In order to determine the linear momentum transfer to the heavy reaction residues, we measured triple coincidences between intermediate mass fragments (Z≈3-13) and angle-correlated binary fission events. The measurements reported here were performed at two IMF angle settings: one backward angle, $\theta_{IMF} = \pm 126°$, which should emphasize ejectiles emitted from an equilibrated target-like source, and one forward angle setting, $\theta_{IMF} = -51°$, which would favor non-equilibrium processes but avoid complications due to projectile fragmentation.

The experiment was performed at the National Superconducting Cyclotron Laboratory at Michigan State University. Angle-correlated fission fragments were detected with two 140 x 140mm^2 x-y position-sensitive multi-wire detectors covering the angular intervals $+59.4° < \theta_A < +110.5°$ and $-115.5° < \theta_B < -64.5°$, respectively. Intermediate mass fragments were detected with standard ΔE-ΔE-E silicon detector telescopes.

The folding angle distribution between coincident binary fission fragments can be related to the average momentum vector, p_R, of the heavy reaction residue through a simple kinematic transformation.[1] We can, therefore, determine the missing momentum,

$$p_m = p_o - p_R - p_{IMF} \cos \theta_{IMF}$$

where p_o and p_{IMF} denote momentum vectors associated with the incident beam momentum and the momentum of the detected fragment, respectively. Missing momenta different from zero result from preequilibrium particle emission or from the sequential decay of highly excited primary fragments. The present experiment cannot distinguish these two mechanisms.

In Fig. 1 fission fragment folding-angle distributions in coincidence with Be, C, O and Ne fragments are shown for the two IMF angle measurements. For comparison the inclusive

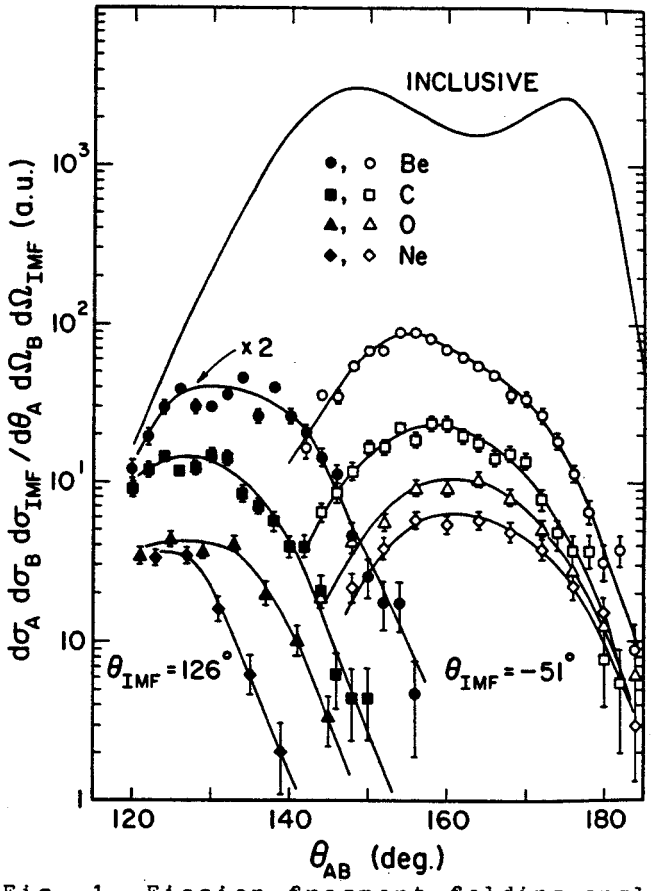

Fig. 1 Fission-fragment folding-angle distributions measured in coincidence with Be, C, O and Ne fragments detected at $\theta_{IMF} = -51°$ (open points) and $\theta_{IMF} = \pm 126°$ (closed points). Solid lines through points are to guide the eye. Upper solid line represents the inclusive folding-angle distribution; its normalization is arbitrary.

fission folding-angle distribution for E/A = 35 MeV ^{14}N ions is also shown on this plot (the cross section normalization between the inclusive and exclusive data is arbitrary). For fixed θ_{IMF}, the folding angle distributions exhibit a monotonic dependence on the atomic number of the detected fragment which is largely due to momentum conservation, see Fig. 2.

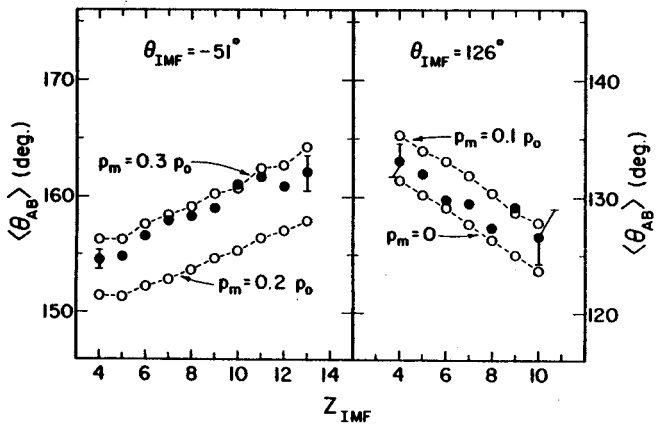

Fig. 2 Average value of the fission fragment folding angle, $\langle\theta_{AB}\rangle$, as a function of coincident ejectile atomic number for the two measured IMF angles. Closed points are experimental values determined recording to Eq. (1). Open points are calculations based on various values of missing momentum, p_m, as described in text.

At θ_{IMF} = 51°, the missing momentum is of the order of 25-30%. The average missing momentum corresponds to 28 ± 3% of the projectile momentum, compared to 42% for the total reaction cross section.[2,3] We estimate average excitation energies of about 320 MeV for sources emitting intermediate mass fragments at θ_{IMF} = 51°. The missing momenta are considerably smaller when intermediate mass fragments are emitted at backward angles, θ_{IMF} = 126°. The average value of $p_m = (0.05 \pm 0.05) \cdot p_0$ indicates that these fragments are emitted in highly inelastic collisions in which nearly the entire momentum of the projectile is transferred to the heavy reaction residue. Within the experimental uncertainties, the emission of intermediate mass fragments at backward angles is consistent with the occurrence of complete fusion of target and projectile, corresponding to an excitation energy deposition of about 420 MeV.

The largest quantitative uncertainty has to be attributed to the unknown effects of sequential decay of highly excited primary reaction products. Since the momenta of undetected decay products are included in our definition of the missing momentum, the occurrence of sequential decay will lead to larger missing momenta when the primary reaction products are emitted at forward angles and to smaller missing momenta when they are emitted at backward angles.

Our results demonstrate that the emission of intermediate mass fragments at backward angles must be attributed to near-equilibrium emission in fusion-like processes in which the missing momentum is surprisingly small when compared to inclusive fusion-like reactions or reactions in which the fragments are emitted at forward angles. These findings suggest that complex fragment emission at backward angles could serve as a reaction filter for the selection of highly excited nuclear systems close to thermal equilibrium.

---

a. Indiana University, Bloomington, IN

References

1. B.B. Back et al., Phys. Rev. C22, 1927 (1980).
2. M.B. Tsang, Phys. Lett. B134, 169 (1984)
3. M. Fatyga et al., Phys. Rev. Lett. 55, 1376 (1985).

NUCLEAR TEMPERATURE MEASUREMENTS AND FEEDING FROM PARTICLE UNBOUND STATES

H.M. Xu, D.J. Fields, W.G. Lynch, M.B. Tsang, C.K. Gelbke, M.R. Maier, D.J. Morrissey, J. Pochodzalla, D.G. Sarantites[a], L.G. Sobotka[a], M.L. Halbert[b], D.C. Hensley[b], D. Hahn[c], and, H. Stöcker[d]

Within the simplifying assumption of local thermal equilibrium, the relative populations of different phase-space configurations may be described by a temperature; the extent of thermalization can then be assessed by measurements of this temperature. Temperatures derived from the slopes of energy spectra may be affected by sensitivities of the spectra to collective motion[1] and to the temporal evolution of the emitting system.[2-4] To a certain extent, these problems may be avoided by extracting "emission temperatures" from the relative populations of ground and excited states of emitted fragments.[5-9]

Recent measurements[5-9] of emission temperatures have provided very different results. The relative populations of particle unstable states of ^{6}Li, ^{5}Li, and ^{8}Be nuclei produced in ^{40}Ar induced reactions on ^{197}Au at E/A=60 MeV[6,8] and in ^{14}N induced reactions on ^{197}Au at E/A=35 MeV[9] are consistent with average emission temperatures of about 4-5 MeV. In contrast, measurements of low energy γ-ray transitions from ^{7}Li, ^{8}Li, and ^{7}Be fragments produced in ^{14}N induced reactions on Ag at E/A=35 MeV yielded emission temperatures of less than 1 MeV.[5,7] These low temperatures were attributed to the breakdown of the approximation of local thermal equilibrium.[5,7] We have measured low energy γ-ray transitions in ^{8}Li, ^{7}Be, ^{10}B, ^{12}B, and ^{13}C nuclei emitted in ^{32}S induced reaction on Ag at 715 MeV and have applied the quantum statistical model[10,11] to estimate the effects of sequential decay.

The experiment was performed at the Holifield Heavy Ion Research Facility of Oak Ridge National Laboratory. Complex fragments with $3 \leq Z \leq 8$ were detected in five ΔE-ΔE-E surface barrier detector telescopes, positioned at the laboratory angles of θ_{lab}=20°, 25°, 30°, 45°, and 50°, with solid angles of $\Delta\Omega_{lab}$= 9.8, 10.1, 15.4, 36.3 and 28.6 msr, respectively. Each telescope consisted of two planar ΔE-detectors with thicknesses between 50 and 100 μm and an E-detector with a thickness of 1.5 mm. Coincident γ-rays were detected with six Compton shielded germanium detector modules of the Spin Spectrometer.[12]

Clean isotopic resolution in the detector telescopes is essential for these measurements. Cross contaminations between adjacent isotopes were reduced to less than 4% by restricting the analysis to fragments that stopped in the third element of the telescope and which simultaneously satisfied two independent particle identification gates.[13] (This double identification requirement introduced energy thresholds at about E/A=8 MeV for θ=20°, 25°, 30° and at about E/A=7 MeV for θ=45° and 50°.) As an example, Fig. 1 shows the measured energy spectra of ^{10}B isotopes. As in previous observations,[4] the fragment energy spectra have maxima near the exit channel Coulomb barrier and decrease exponentially with increasing fragment energy; the cross sections are strongly enhanced at forward angles. Moving source analyses of the kinetic energy spectra suggest that at least half of the fragments are emitted prior to complete equilibration of the composite system.[14]

The energy spectra of coincident γ-rays were transformed into the rest frames of the coincident particles using relativistic Jacobians and Doppler shift corrections. Since

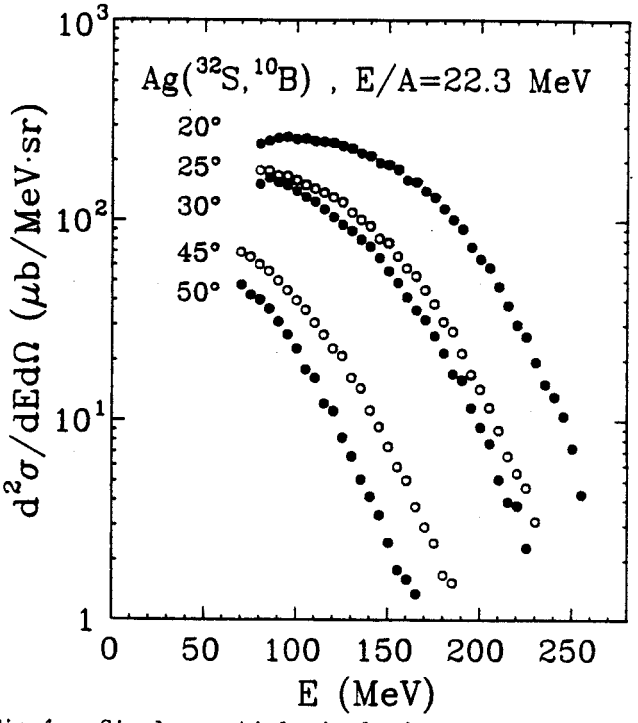

Fig.1. Single particle inclusive cross sections for ^{10}B nuclei emitted in ^{32}S induced reactions on Ag at E/A=22.3 MeV.

these transformations shift and broaden γ-ray transitions of the target residues, particular attention was paid to identifying and correcting for spurious structures in the γ-ray background. For this purpose, background spectra were generated by performing similar Doppler shift transformations on raw γ-ray spectra measured in coincidence with ^{6}Li, ^{9}Be, and ^{11}B nuclei. These nuclei have no strong γ-ray transitions at the γ-ray energies studied here; however, these background spectra contained discrete transitions from target residues common to all spectra.

Spectra of γ-rays detected in coincidence with isotopes of ^{8}Li, ^{7}Be, ^{10}B, ^{12}B, and ^{13}C are shown by the histograms in Fig. 2. The Doppler shifted background spectra are indicated by the solid dots in the figure. The following transitions were analyzed: ^{8}Li($J^{\pi}=1^{+}$, $E^{*}=0.981$ MeV → $J^{\pi}=2^{+}$, $E^{*}=0.0$ MeV), ^{7}Be($\frac{1}{2}^{-}$, 0.429 → $\frac{3}{2}^{-}$, 0.0), ^{10}B(1^{+}, 2.154 → 0^{+}, 1.740), ^{13}C($\frac{5}{2}^{+}$, 3.854 → $\frac{3}{2}^{-}$, 3.684), and overlapping transitions: ^{12}B(2^{+}, 0.953 → 1^{+}, 0.0), ^{12}B(1^{-}, 2.621 → 2^{-}, 1.674). We did not analyze the transition, ^{7}Li($\frac{1}{2}^{-}$, 0.478 → $\frac{3}{2}^{-}$, 0.0), because the pile-up of two coincident α-particles in the telescopes is misidentified as a ^{7}Li[15], nor the long-lived transition, ^{10}B(1^{+}, 0.718 → 3^{+}, 0.0; τ=1.02 ns)[16], because this decay occurs at a considerable distance from the target resulting in major uncertainties in the efficiencies of the γ-ray detectors. The data in Fig. 2 were summed over all detectors; the individual detectors provide comparable numerical contributions to the sum. The inclusive fragment yields and fragment-γ-ray coincidence yields were summed over angle and combined to extract the fraction[5,7], F_{γ}, of observed fragments which were accompanied by the designated γ-ray. Spin alignments were assumed

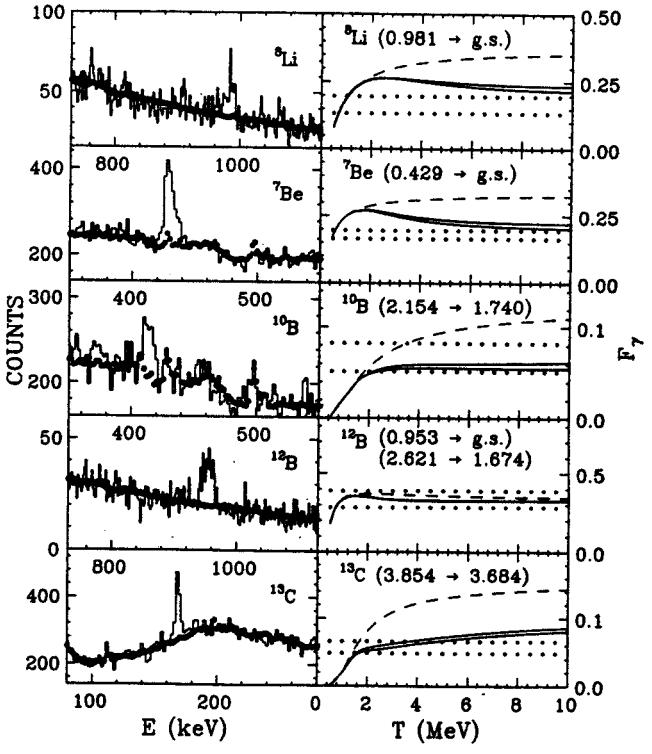

Fig. 2. Left hand side: γ-ray spectra for ^{8}Li, ^{7}Be, ^{10}B, ^{12}B, and ^{13}C isotopes produced in ^{32}S induced reactions Ag at E/A=22.3 MeV. Right hand side: fractional probabilities, F_{γ}, that an observed fragment is accompanied by the designated γ-ray. Dotted lines denote the range of values for F_{γ} consistent with the coincidence measurements. Dashed and solid curves are discussed in the text.

Table 1: Fractional probabilities, F_γ, that the observed fragment is accompanied by the designated γ-ray.

Fragment	Transition	F_γ
^{8}Li	1^+, 0.981 → 2^+, 0.0	0.165±0.032
^{7}Be	$\frac{1}{2}^-$, 0.429 → $\frac{3}{2}^-$, 0.0	0.180±0.016
^{10}B	1^+, 2.154 → 0^+, 1.740	0.067±0.015
^{12}B	2^+, 0.953 → 1^+, 0.0	0.336±0.053
	1^-, 2.621 → 2^-, 1.674	
^{13}C	$\frac{5}{2}^+$, 3.854 → $\frac{3}{2}^-$, 3.684	0.057±0.009

to be zero. This introduced a spin alignment dependent uncertainty in F_γ of about 3%. Values of F_γ for these transitions are given in Table 1.

To assess the magnitude of the sequential decay corrections, we have calculated F_γ with the quantum statistical model[10,11] which has been used to describe fragmentation in energetic nucleus-nucleus collisions.[17] The calculation proceeds in two stages: i) the initial populations of states of particle stable and unstable fragments are calculated by solving equations of chemical equilibrium for nuclear matter at uniform breakup density[18], ρ, and temperature, T; ii) the excited states decay[19] sequentially to fragments with larger binding energies according to available information[16] concerning the spins and branching ratios of each excited state.

We first discuss the calculations for F_γ in which sequential feeding from particle unstable states of heavier nuclei is neglected and only the feeding from higher lying γ-unstable excited states of the same nucleus is considered. Values for F_γ consistent with this approximation are shown by the dashed lines in the right hand side of Fig. 2. The dotted lines indicate the upper and lower limits for F_γ consistent with our measurements. If sequential decay were neglected[5,7], temperatures of 0.5±0.1 MeV, 0.9±0.3 MeV, 2.4±0.8 MeV, and 1.6±0.2 MeV would be extracted from the transitions in ^{7}Be, ^{8}Li, ^{10}B, and ^{13}C, respectively. These temperatures are mutually inconsistent. Higher temperatures are extracted for transitions from states with higher excitation energy. This trend can be expected when secondary processes, such as sequential decay, modify the primary populations of ground and excited states.[6]

The full calculations, which include sequential feeding from particle unbound states, are shown in the right hand side of Fig. 2 for densities $0.3\rho_o$ (upper solid line) and $0.7\rho_o$ (lower solid line), where ρ_o denotes normal nuclear matter density. Sequential decay reduces considerably the theoretical values for F_γ bringing them close to the experimental values. For ^{7}Be, ^{8}Li, and ^{12}B nuclei, the dependence of F_γ on temperature is even predicted to be non-monotonic. Only at very low temperatures, T≤1-1.3 MeV, can sequential decay be neglected for the calculation of F_γ. At very low bombarding energies where this neglect may be justified, emission temperatures are consistent with the temperature of the equilibrated compound nucleus provided the compound nuclear temperature is less than 1.5 MeV.[20] At higher bombarding energies corresponding to higher compound nuclear temperatures, however, the experimental F_γ values are smaller than those predicted for negligible feeding; thus, emission temperatures were obtained which were considerably smaller than the temperature of the compound nucleus.[20] Our statistical model calculations show that this trend is mainly due to the increased importance of sequential feeding at the higher bombarding energies.

At temperatures greater than 2 MeV, we estimate an uncertainty of at least 25% in the theoretical values of F_γ arising from our present incomplete understanding of the fragmentation process and due to the lack of information concerning the spins and branching

ratios for many of the tabulated[16] particle unstable states. Within this uncertainty, the full calculations, at $T \geq 4$ MeV, are consistent with the experimental measurements. Theoretical uncertainties and the insensitivity of the theoretical values of F_γ to temperature prevent the extraction of meaningful emission temperatures, for $T \geq 2$ MeV, from these low energy γ-ray transitions. The calculations are nonetheless capable of indicating whether specific transitions are strongly influenced by sequential feeding. In particular, these and other statistical calculations show that the relative populations of particle unstable states presented in ref. 6, 8, and 9 are relatively insensitive to sequential decay at temperatures less than 4 MeV.[6,21] Although sequential decay may strongly influence the relative populations of ^{6}Li and ^{8}Be particle unstable states at higher temperatures, the relative populations of states in ^{5}Li are predicted to be relatively unperturbed by secondary decays for temperatures as large as 10 MeV.[6,21]

---

a. Department of Chemistry, Washington University, St. Louis, MO 63130
b. Physics Division, Oak Ridge National Laboratory, Oak Ridge, TN 37830
c. Lawrence Berkeley Laboratory, Berkeley CA 94720.
d. Institut für Theoretische Physik, J.W. Goethe Universität, Frankfurt am Main, Germany.

References

1. P.J. Siemens and J.O. Rasmussen, Phys. Rev. Lett. 42 (1979) 880.
2. H. Stöcker, et al., Z. Phys. A303 (1981) 259.
3. W.A. Friedman and W.G. Lynch, Phys. Rev. C28 (1983) 16.
4. D.J. Fields, et al., Phys. Rev. C30 (1984) 1912.
5. D.J. Morrissey, et al., Phys. Lett. B148 (1984) 423.
6. J. Pochodzalla, et al., Phys. Rev. Lett. 55 (1985) 177.
7. D.J. Morrissey, et al., Phys. Rev. C32 (1985) 877.
8. J. Pochodzalla, et al., Phys. Lett. B161 (1985) 275.
9. C.B. Chitwood, et al., Phys. Lett. B172 (1986) 27.
10. H. Stöcker, et al., Nucl. Phys. A400 (1983) 63c.
11. D. Hahn and H. Stöcker, to be published
12. M. Jääskeläinen, et al., Nucl. Instr. Meth. 204 (1983) 385.
13. N. Anyas-Weiss, et al, Phys. Reports 12c (1974) 201.
14. D.J. Fields, et al., Phys. Rev. C, in press.
15. G.J. Wozniak, et al., Nucl. Instr. and Meth. 120 (1974) 29.
16. F. Ajzenberg-Selove, Nucl. Phys. A449 (1986) 1.
17. B.V. Jacak, et al., Phys. Rev. Lett. 51 (1983) 1846.
18. The ratio of the proton density to the neutron density was chosen to be .82, consistent with the compound nucleus.
19. W. Hauser and H. Feshbach, Phys. Rev. 87 (1952) 366.
20. D.J. Morrissey, et al., Phys. Rev. C, in press.
21. D.J. Fields, et al., to be published.